

## PARAMETERIZATION OF $\gamma$ , $e^\pm$ , AND NEUTRINO SPECTRA PRODUCED BY $p$ - $p$ INTERACTION IN ASTRONOMICAL ENVIRONMENTS

TUNEYOSHI KAMAE,<sup>1</sup> NIKLAS KARLSSON,<sup>2</sup> TSUNEFUMI MIZUNO,<sup>3</sup> TOSHINORI ABE,<sup>4</sup> AND TATSUMI KOI  
Stanford Linear Accelerator Center, Menlo Park, CA 94025; kamae@slac.stanford.edu  
Received 2005 December 9; accepted 2006 April 6

### ABSTRACT

We present the yield and spectra of stable secondary particles ( $\gamma$ ,  $e^\pm$ ,  $\nu_e$ ,  $\bar{\nu}_e$ ,  $\nu_\mu$ , and  $\bar{\nu}_\mu$ ) of  $p$ - $p$  interaction in parameterized formulae to facilitate calculations involving them in astronomical environments. The formulae are derived from the up-to-date  $p$ - $p$  interaction model by Kamae et al. (2005), which incorporates the logarithmically rising inelastic cross section, the diffraction dissociation process, and the Feynman scaling violation. To improve fidelity to experimental data in lower energies, two baryon resonance contributions have been added: one representing  $\Delta(1232)$  and the other representing multiple resonances around 1600 MeV/ $c^{-2}$ . The parameterized formulae predict that all secondary particle spectra be harder by about 0.05 in power-law indices than that of the incident proton and their inclusive cross sections be larger than those predicted by  $p$ - $p$  interaction models based on the Feynman scaling.

*Subject headings:* cosmic rays — galaxies: jets — gamma rays: theory — ISM: general — neutrinos — supernovae: general

*Online material:* source code

### 1. INTRODUCTION

Gamma-ray emission due to neutral pions produced by proton-proton interaction has long been predicted from the Galactic ridge, supernova remnants (SNRs), active galactic nucleus (AGN) jets, and other astronomical sites (Hayakawa 1969; Stecker 1971; Murthy & Wolfendale 1986; Schönfelder 2001; Schlickeiser 2002; Aharonian 2004; Aharonian et al. 2004). High-energy neutrinos produced by  $p$ - $p$  interaction in AGN jets will soon be detected with large-scale neutrino detectors that are under construction (Halzen 2005). Spectra of these gamma rays, neutrinos, and other secondaries depend heavily on the incident proton spectrum, which is unknown and needs to be derived, in almost all cases, from the observed spectra themselves. Such analyses often involve iterative calculations with many trial proton spectra. The parameterized model presented here is aimed to improve accuracy of such calculations.

Among the secondaries of  $p$ - $p$  interaction in an astronomical environment, gamma rays have been best studied. The  $p$ - $p$  interaction is one of the two dominant gamma-ray emission mechanisms in the sub-GeV to multi-TeV range, the other being Compton up-scattering of low-energy photons by high-energy electrons. Gamma rays in this energy range have been detected from pulsars, the Galactic ridge, SNRs, blazars, and other source categories (Stecker 1971; Murthy & Wolfendale 1986; Ong 1998; Schönfelder 2001; Weekes 2003; Aharonian 2004).

High-energy gamma rays from AGN jets are interpreted as mostly due to the inverse Compton up-scattering of low-energy photons by multi-TeV electrons. Observed radio and X-ray spectra match those of synchrotron radiation by these electrons. Synchronicity in variability between the observed X-ray and gamma-ray fluxes has given strong support for the inverse

Compton up-scattering scenario (Ong 1998; Schönfelder 2001; Schlickeiser 2002; Aharonian 2004). For some AGN jets, the above scenario does not work well, and  $p$ - $p$  interaction has been proposed as an alternative mechanism (Mücke & Protheroe 2001; Mücke et al. 2003; Böttcher & Reimer 2004).

High-energy gamma rays detected by COS-B and EGRET from the Galactic ridge, on the other hand, are interpreted as predominantly due to neutral pions produced by the interaction of protons and nuclei with the interstellar matter (ISM; Stecker 1973; Strong et al. 1978, 1982, 2000; Stephens & Badhwar 1981; Mayer-Hasselwander et al. 1982; Bloemen et al. 1984; Bloemen 1985; Dermer 1986a; Stecker 1990; Hunter et al. 1997; Mori 1997; Stanev 2004). The measured gamma-ray flux and spectral shape (Hunter et al. 1997) have been viewed as the key attestation to this interpretation. It is also known that inverse Compton scattering contributes significantly to the Galactic ridge gamma-ray emission (Murthy & Wolfendale 1986; Strong et al. 2000; Schönfelder 2001).

In the past two years, several SNRs, including RX J1713–3946 and RX J0852–4622, have been imaged in the TeV band with an angular resolution around  $0.1^\circ$  by H.E.S.S. (Aharonian et al. 2004b, 2004c; Aharonian 2005). A smooth featureless spectrum, suggestive of synchrotron radiation by multi-TeV electrons, has been detected in the X-ray band from RX J1713–3946 (Koyama et al. 1997; Slane et al. 1999; Uchiyama et al. 2003) and RX J0852–4622 (Tsunemi et al. 2000; Iyudin et al. 2005). The measured TeV gamma-ray fluxes and spectra, however, do not agree well with those predicted by the inverse Compton scenario (see, e.g., the analysis in Uchiyama et al. 2003). Several authors have proposed that the TeV gamma rays are possibly due to the interaction of accelerated protons with the ISM (Berezhko & Volk 2000; Enomoto et al. 2002; Aharonian 2004; Katagiri et al. 2005).

Higher precision data are expected, in the GeV range, from the GLAST Large Area Telescope (GLAST-LAT 2005)<sup>5</sup> and, in the TeV range, from the upgraded Air Cerenkov Telescopes (Aharonian et al. 2004); they will soon test applicability of the inverse Compton up-scattering and the proton interaction with

<sup>1</sup> Also with Kavli Institute for Particle Astrophysics and Cosmology, Stanford University, Menlo Park, CA 94025.

<sup>2</sup> Visiting scientist from Royal Institute of Technology, SE-10044 Stockholm, Sweden.

<sup>3</sup> Current address: Department of Physics, Hiroshima University, Higashi-Hiroshima 739-8511, Japan.

<sup>4</sup> Current address: Department of Physics, University of Tokyo, Tokyo 113-0033, Japan.

<sup>5</sup> GLAST Large Area Telescope, <http://www-glast.stanford.edu>.

ISM for various astronomical gamma-ray sources. In many objects, secondary electrons and positrons may produce fluxes of hard X-rays and low-energy gamma rays detectable with high-sensitivity instruments aboard *INTEGRAL*, *Swift*, *Suzaku*, and *NuSTAR*.<sup>6</sup> The formulae given here will give fluxes and spectra of these secondary particles for arbitrary incident proton spectrum.

This work is an extension of that by Kamae et al. (2005), where up-to-date knowledge of the  $\pi^0$  yield in the  $p$ - $p$  inelastic interaction has been used to predict the Galactic diffuse gamma-ray emission. The authors have found that past calculations (Stecker 1970, 1973, 1990; Strong et al. 1978; Stephens & Badhwar 1981; Dermer 1986a, 1986b, 2000; Mori 1997) had left out the diffractive interaction and the Feynman scaling violation in the nondiffractive inelastic interaction. Another important finding by them is that most previous calculations have assumed an energy-independent  $p$ - $p$  inelastic cross section of about 24 mbarn for  $T_p \gg 10$  GeV, whereas recent experimental data have established a logarithmic increase with the incident proton energy. Updating these shortfalls has changed the prediction of the gamma-ray spectrum in the GeV band significantly: the gamma-ray power-law index is harder than that of the incident proton, and the GeV–TeV gamma-ray flux is significantly larger than that predicted on the constant cross section and Feynman scaling (Kamae et al. 2005). The model by Kamae et al. (2005) will hereafter be referred to as model A.

Model A does not model  $p$ - $p$  interaction accurately near the pion production threshold. To improve prediction of gamma rays, electrons, and positrons produced near the pion production threshold, two baryon resonance excitation components have been added to model A:  $\Delta(1232)$ , representing the  $\Delta$  resonance, and  $\text{res}(1600)$ , representing resonances around 1600 MeV/ $c^2$ . We note here that  $\Delta(1232)$  is the most prominent and lightest baryon resonance excited in the  $p$ - $p$  interaction. It has a mass of 1.232 GeV/ $c^2$  and a width of about 0.12 GeV/ $c^2$ , and decays to a nucleon (proton or neutron) and a pion ( $\pi^{+,0,-}$ ). The other resonance,  $\text{res}(1600)$ , is assumed to decay to a nucleon and two pions. Introduction of these contributions has necessitated adjustment of model A at lower energies, as described below. The readjusted model will be referred to as the “readjusted model A.”

The parameterized model presented here exhibits all features of model A at higher energies (proton kinetic energy,  $T_p > 3$  GeV) and reproduces experimental data down to the pion production threshold. The inclusive gamma-ray and neutrino cross section formulae can be used to predict their yields and spectra for a wide range of incident proton spectrum. Formulae for electrons and positrons predict sub-TeV to multi-TeV secondary electrons and positrons supplied by  $p$ - $p$  interaction. We note that space-borne experiments such as PAMELA<sup>7</sup> will soon measure the electron and positron spectra in the sub-TeV energy range, where the secondaries of  $p$ - $p$  interaction may become comparable to the primary components (Müller 2001; Stephens 2001; DuVernois et al. 2001).

Due to paucity of experimental data and widely accepted modeling, we have not parameterized inclusive secondary cross sections for  $\alpha$ - $p$ ,  $p$ -He, or  $\alpha$ -He interactions. We note that  $\alpha$ -particles are known to make up about 7% by number of cosmic rays observed near the Earth (Schlickeiser 2002) and He to make up  $\sim 10\%$  by number of interstellar gas. The total non  $p$ - $p$  contribution is comparable to that of the  $p$ - $p$  contribution. The  $\alpha$ -particle and He nucleus can be regarded, to a good approximation, as four independent protons beyond the resonance region ( $T_p > 3$  GeV);

the error introduced is expected to be less than 10% for high-energy light secondary particles (Kamae et al. 2005).

Inclusion of  $\alpha$ -particles as projectiles and He nuclei as targets will change the positron–electron ratio significantly (about 10%–15%), as discussed below. Fermi motion of nucleons and multiple nucleonic interactions in the nucleus are known to significantly affect pion production near the threshold and in the resonance region ( $T_p < 3$  GeV; Crawford et al. 1980; Mårtensson et al. 2000); we acknowledge the need for separate treatment of  $p$ -He,  $\alpha$ - $p$ , and  $\alpha$ -He interactions in the future.

## 2. MONTE CARLO EVENT GENERATION

The parameterization of the inclusive cross sections for  $\gamma$ ,  $e^\pm$ ,  $\nu$ , and  $\bar{\nu}$  has been carried out, separately, for nondiffractive, diffractive, and resonance–excitation processes, in three steps: First, the secondary particle spectra have been extracted out of events generated for monoenergetic protons (0.488 GeV  $< T_p < 512$  TeV) based on the readjusted model A. We then fit these spectra with a common parameterized function, separately for nondiffractive, diffractive, and resonance–excitation processes. In the third step, the parameters determined for monoenergetic protons are fitted as functions of proton energy, again separately for the three processes. The above procedure has been repeated for all secondary particle types.

The functional formulae often introduce tails extending beyond the energy-momentum conservation limits, which may produce artifacts when wide-range spectral energy density [ $E^2 d\text{flux}(\gamma)/dE$ ] is plotted. To eliminate such artifacts, we introduce another set of functions to impose the kinematic limits.

Several simulation programs have been used in model A (Kamae et al. 2005): for the high-energy nondiffractive process ( $T_p > 52.6$  GeV), Pythia 6.2 (Sjöstrand et al. 2001) with the multiparton-level scaling violation option (Sjöstrand & Skands 2004);<sup>8</sup> for the lower energy nondiffractive process, the parameterized model by Blatnig et al. (2000); and for the diffractive part, the program by T. Kamae (2004, personal communication).<sup>9</sup> In the readjusted model A, two programs to simulate two resonance–excitation components have also been added. Modeling of the two resonance components will be explained below.

## 3. NONDIFFRACTIVE, DIFFRACTIVE, AND RESONANCE-EXCITATION CROSS SECTIONS

Experimental data on  $p$ - $p$  cross sections are archived for a broad range of the incident proton energy and various final states. The total and elastic cross sections have been compiled from those by Hagiwara et al. (2002), as shown in Figure 1. The two thin curves running through experimental data points in the figure are our by-eye fits to the total and elastic cross sections. We then define the “empirical” inelastic cross section as the difference of the two curves to which the sum of nondiffractive, diffractive,  $\Delta(1232)$ -excitation, and  $\text{res}(1600)$ -excitation components are constrained. Typical errors in the empirical inelastic cross section are 20% for  $T_p < 3$  GeV and 10% for  $T_p > 3$  GeV.

The four component cross sections of the readjusted model A and their sum are shown in Figures 1 and 2. The empirical inelastic cross section is shown by a series of small circles in Figure 2. The component cross sections take formulae given in equations (1) (nondiffractive), (2) (diffractive), (3) [ $\Delta(1232)$ ], and (4) [ $\text{res}(1600)$ ] and numerical values given in Table 1. These are also shown in Figures 1 and 2.

We note that there is no clear experimental method separating the four components, especially at lower energies ( $T_p < 20$  GeV).

<sup>6</sup> See *INTEGRAL* Web site, <http://sci.esa.int/esaMI/Integral>, the *NuSTAR* Web site, <http://www.nustar.caltech.edu>, the *Suzaku* Web site, <http://www.isas.jaxa.jp/e/enterp/missions/astro-e2>, and the *Swift* Web site, <http://swift.gsfc.nasa.gov/docs/swift>.

<sup>7</sup> See <http://wizard.roma2.infn.it/pamela>.

<sup>8</sup> See <http://cepa.fnal.gov/CPD/MCTuning1> and <http://www.phys.ufl.edu/~rfield/cdf>.

<sup>9</sup> Diffractive process has been included in Pythia after the work began.

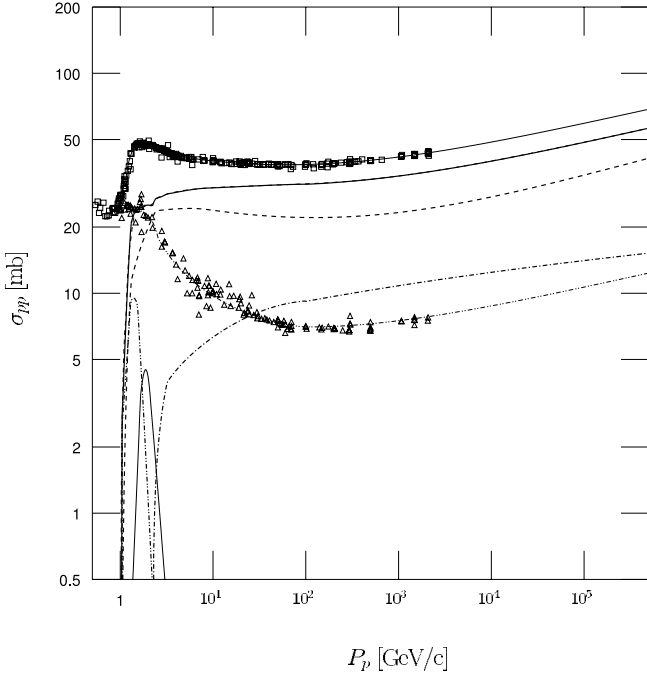


FIG. 1.—Experimental  $p$ - $p$  cross sections, as a function of proton momentum, and that of readjusted model A: experimental total (squares), experimental elastic (triangles), total inelastic (thick solid line), nondiffractive process (dashed line), diffractive process (dot-dashed line),  $\Delta(1232)$  (dotted line), and  $\text{res}(1600)$  (thin solid line). The total inelastic is the sum of the four components. The thin solid and double-dot-dashed lines running through the two experimental data sets are by-eye fits to the total and elastic cross sections, respectively.

This ambiguity does not significantly affect the secondary particle fluxes, as long as the sum agrees with the total inelastic cross section and the total secondary inclusive cross sections agree with the corresponding experimental data.

The secondary particle spectra for a monoenergetic proton are normalized to the component cross sections given in equations (1), (2), (3), and (4) at the corresponding proton energy. We note that the nondiffractive component for  $T_p < 52.6$  GeV is based on the formula by Blattnig et al. (2000), which is normalized to their  $\pi^0$  inclusive cross section formula, not to the total inelastic cross section. In the readjusted model A, this component cross section is defined by equation (1), and the  $\pi^0$  inclusive cross section formula of Blattnig et al. (2000) has been redefined so that the sum of the four components reproduces the experimental  $\pi^0$  inclusive cross section. The positive and negative pion inclusive cross sections are also redefined as products of our  $\pi^0$  inclusive cross section and the ratio of the  $\pi^{+,-}$  and  $\pi^0$  inclusive cross sections given in Blattnig et al. (2000):

$$\sigma_{\text{nondiff}}^{pp}(x)[\text{mbarn}] = \begin{cases} 0 & P_p < 1 \text{ GeV}/c, \\ a_0(x/a_1)^{1.2} \{a_2 + a_3x^2 + a_4x^3 + a_5 \exp[-a_6(x+a_7)^2]\} & 1 \leq P_p \leq 1.3 \text{ GeV}/c, \\ \frac{(b_0|a_1 - x| + b_1|a_0 - x|)}{(a_1 - a_0)} & 1.3 \leq 1.3P_p \leq 2.4 \text{ GeV}/c, \\ a_2 + a_3x^2 + a_4x^3 + a_5 \exp[-a_6(x+a_7)^2] & 2.4 \leq P_p \leq 10 \text{ GeV}/c, \\ c_0 + c_1x + c_2x^2 & P_p > 10 \text{ GeV}/c, \end{cases} \quad (1)$$

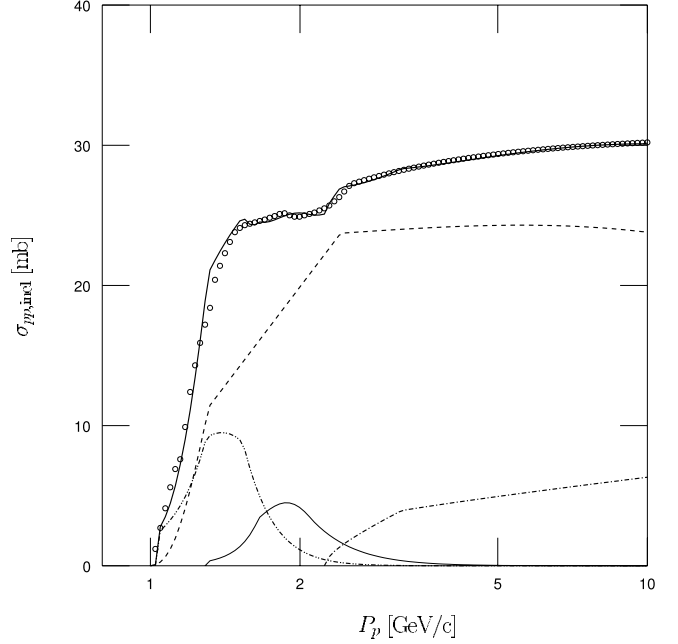


FIG. 2.—Experimental  $p$ - $p$  cross sections, as a function of proton momentum, and that of readjusted model A for  $T_p < 10$  GeV. Small circles represent the empirical inelastic cross section described in the text. Lines are the same as in Fig. 1.

$$\sigma_{\text{diff}}^{pp}(x)[\text{mbarn}] = \begin{cases} 0 & P_p < 2.25 \text{ GeV}/c, \\ \sqrt{(x-d_0)/d_1} \times \{d_2 + d_3 \log[d_4(x-0.25)] + d_5x^2 - d_6x^3\} & 2.25 \leq P_p \leq 3.2 \text{ GeV}/c, \\ d_2 + d_3 \log[d_4(x-0.25)] + d_5x^2 - d_6x^3 & 3.2 \leq P_p \leq 100 \text{ GeV}/c, \\ e_0 + e_1x & P_p > 100 \text{ GeV}/c, \end{cases} \quad (2)$$

$$\sigma_{\Delta(1232)}^{pp}(x)[\text{mbarn}] = \begin{cases} 0 & P_p < 1.4 \text{ GeV}/c, \\ f_0 E_p^{10} & 1.4 \leq P_p \leq 1.6 \text{ GeV}/c, \\ f_1 \exp[-f_2(E_p - f_3)^2] & 1.6 \leq P_p \leq 1.8 \text{ GeV}/c, \\ f_4 E_p^{-10} & 1.8 \leq P_p \leq 10 \text{ GeV}/c, \\ 0 & P_p > 10 \text{ GeV}/c, \end{cases} \quad (3)$$

$$\sigma_{\text{res}(1600)}^{pp}(x)[\text{mbarn}] = \begin{cases} 0 & P_p < 1.6 \text{ GeV}/c, \\ g_0 E_p^{14} & 1.6 \leq P_p \leq 1.9 \text{ GeV}/c, \\ g_1 \exp[-g_2(E_p - g_3)^2] & 1.9 \leq P_p \leq 2.3 \text{ GeV}/c, \\ g_4 E_p^{-6} & 2.3 \leq P_p \leq 20 \text{ GeV}/c, \\ 0 & P_p > 20 \text{ GeV}/c, \end{cases} \quad (4)$$

where  $x = \log(P_p[\text{GeV}/c])$  and  $E_p$  is the proton energy in GeV.

### 3.1. Introduction of Resonance-Excitation Processes to Model A

One or both of the projectile and target protons can be excited to baryon resonances in the  $p$ - $p$  interaction. Here we use “baryon

TABLE I  
CONSTANTS FOR EQUATIONS (1), (2), (3), AND (4)

Parameter $a$	$b$	$c$	$d$	$e$	$f$	$g$
$a_0 = 0.57$	$b_0 = 11.34$	$c_0 = 28.5$	$d_0 = 0.3522$	$e_0 = 5.922$	$f_0 = 0.3433$	$g_0 = 0.005547$
$a_1 = 0.01176$	$b_1 = 23.72$	$c_1 = -6.133$	$d_0 = 0.1530$	$e_1 = 1.632$	$f_1 = 9.5$	$g_1 = 4.5$
$a_2 = 23.10$		$c_2 = -1.464$	$d_2 = 1.498$		$f_2 = -5.5$	$g_2 = -7.0$
$a_3 = 6.454$			$d_3 = 2.0$		$f_3 = 1.68$	$g_3 = 2.1$
$a_4 = -5.764$			$d_4 = 30.0$		$f_4 = 3134$	$g_4 = 14089$
$a_5 = -23.63$			$d_5 = 3.155$			
$a_6 = 94.75$			$d_6 = 1.042$			
$a_7 = 0.02667$						

resonances” to represent both nucleon resonances (iso-spin = 1/2) and  $\Delta$  resonances (iso-spin = 3/2). These excitations enhance the pion production (and hence secondary particle production) near the inelastic threshold. The most prominent resonance among them is  $\Delta(1232)$ , which has a mass of 1232 MeV/ $c^2$  and decays predominantly (>99%) to a nucleon and a pion (Hagiwara et al. 2002).

Stecker (1970) proposed a cosmic gamma-ray model in which neutral pions are produced only through the  $\Delta(1232)$  excitation for  $T_p \leq 2.2$  GeV. The resonance is assumed to move only in the direction of the incident proton. At higher energies, another process, the fireball process, sets in and produces pions with limited transverse momenta.

Dermer (1986a) compared predictions of models on  $\pi^0$  kinetic energy distribution in the proton-proton center-of-mass (CM) system with experiments and noted that the model by Stecker (1970) reproduces data better than the scaling model by Stephens & Badhwar (1981) for  $T_p < 3$  GeV. He proposed a cosmic gamma-ray production model that covers a wider energy range by connecting the two models in the energy range  $T_p = 3-7$  GeV.

Model A by Kamae et al. (2005) has been constructed primarily for the  $p$ - $p$  inelastic interaction  $T_p \gg 1$  GeV and has left room for improvement for  $T_p < 3$  GeV. The diffraction disso-

ciation component of model A has a resonance-excitation feature similar to that implemented in Stecker (1971) for  $T_p > 3$  GeV, where either or both protons can be excited to nucleon resonances (iso-spin = 1/2 and mass around 1600 MeV/ $c^2$ ) along the direction of the incident and/or target protons. What has not been implemented in model A is the enhancement by baryon resonances in the inclusive pion production cross sections below  $T_p < 3$  GeV.

We note here that the models by Stecker (1970) and by Dermer (1986a; see also Dermer 1986b) used experimental data on the inclusive  $\pi^0$  yield (and that of charged pions) to guide their modeling, but not the total inelastic cross section. Model A by Kamae et al. (2005), on the other hand, has simulated all particles in each event (referred to as the “exclusive” particle distribution) for all component cross sections. One exception is the simulation of the low-energy nondiffractive process ( $T_p < 52.6$  GeV) by Blattnig et al. (2000). The inclusive  $\pi^0$  (or gamma-ray) yield is obtained by collecting  $\pi^0$  (or gamma rays) in simulated exclusive events. When readjusting model A by adding the resonance-excitation feature similar to that by Stecker (1970), overall coherence to model A has been kept. We adjusted the  $\Delta(1232)$  excitation cross section to reproduce the total inelastic cross section given in Figure 2 and fixed the average pion multiplicities for + : 0 : - to those expected by the one-pion-exchange

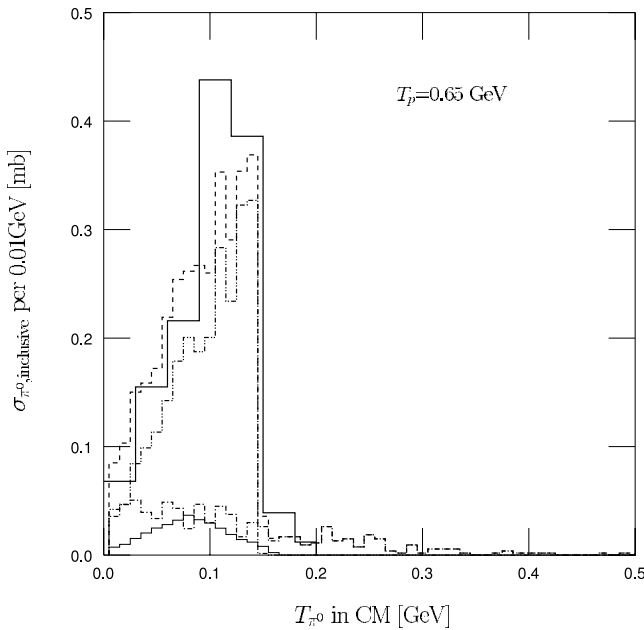


FIG. 3.—Experimental and simulated  $\pi^0$  kinetic energy distributions in the  $p$ - $p$  CM system for  $T_p = 0.65$  GeV. The thick solid line is the experimental data taken from Fig. 3 of Dermer (1986a). The dashed line is the sum of all readjusted model A components: nondiffractive (dot-dashed line),  $\Delta(1232)$  (double-dot-dashed line), and res(1600) (thin solid line).

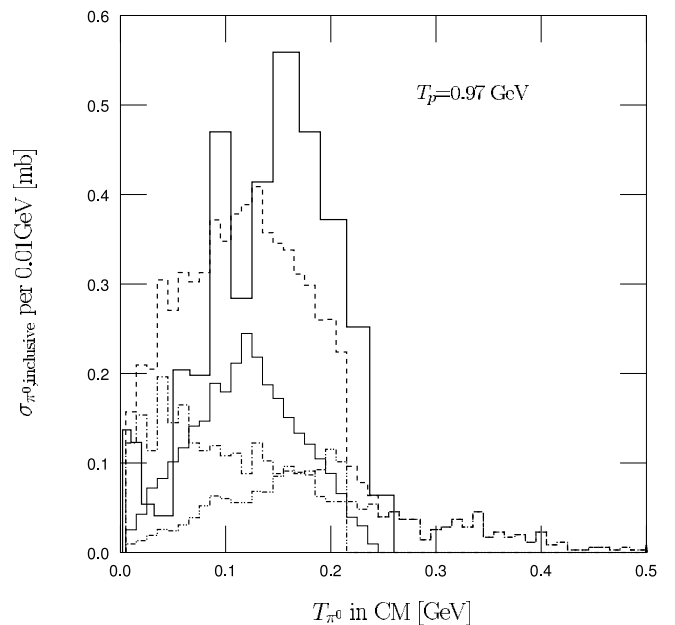


FIG. 4.—Experimental and simulated  $\pi^0$  kinetic energy distributions in the  $p$ - $p$  CM system for  $T_p = 0.97$  GeV. The thick solid line represents experimental data (taken from Fig. 4 of Dermer 1986a). Other lines are the same as in Fig. 3.

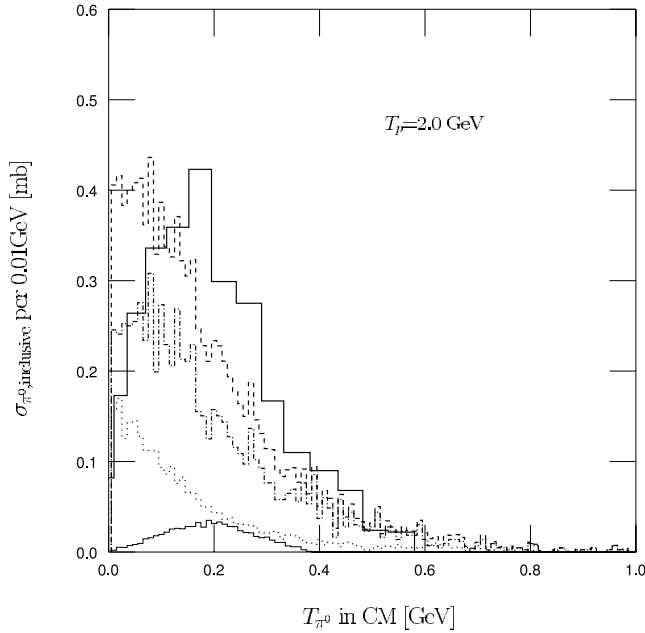


FIG. 5.—Experimental and simulated  $\pi^0$  kinetic energy distribution in the  $p$ - $p$  CM system for  $T_p = 2.0$  GeV. The thick solid line represents experimental data (taken from Fig. 5 of Dermer 1986a), and the dotted line is for the diffractive process. The others are the same as in Fig. 3.

hypothesis,  $0.73 : 0.27 : 0.0$ . As higher mass resonances begin to contribute, the average pion multiplicity is expected to increase. To reproduce the experimental  $\pi^0$  inclusive cross section and total inelastic cross section for  $T_p < 3$  GeV, we introduced a second resonance,  $\text{res}(1600)$ . This resonance does not correspond to any specific resonance but represents several baryon resonances at

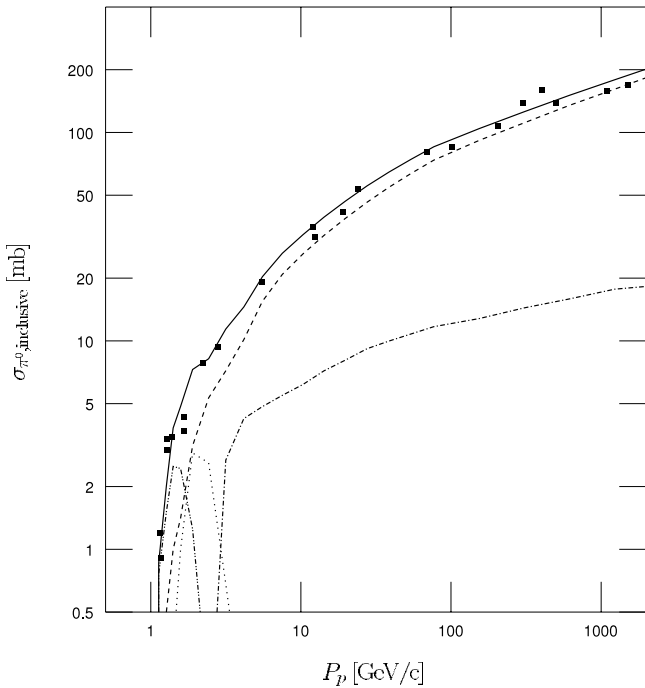


FIG. 6.—Experimental and simulated  $\pi^0$  inclusive cross section. Experimental data are those assembled by Stecker (1970) and Dermer (1986a). Lines are those of readjusted model A: total (solid line), nondiffractive (dashed line), diffractive process (dot-dashed line),  $\Delta(1232)$  (double-dot-dashed line), and  $\text{res}(1600)$  (dotted line).

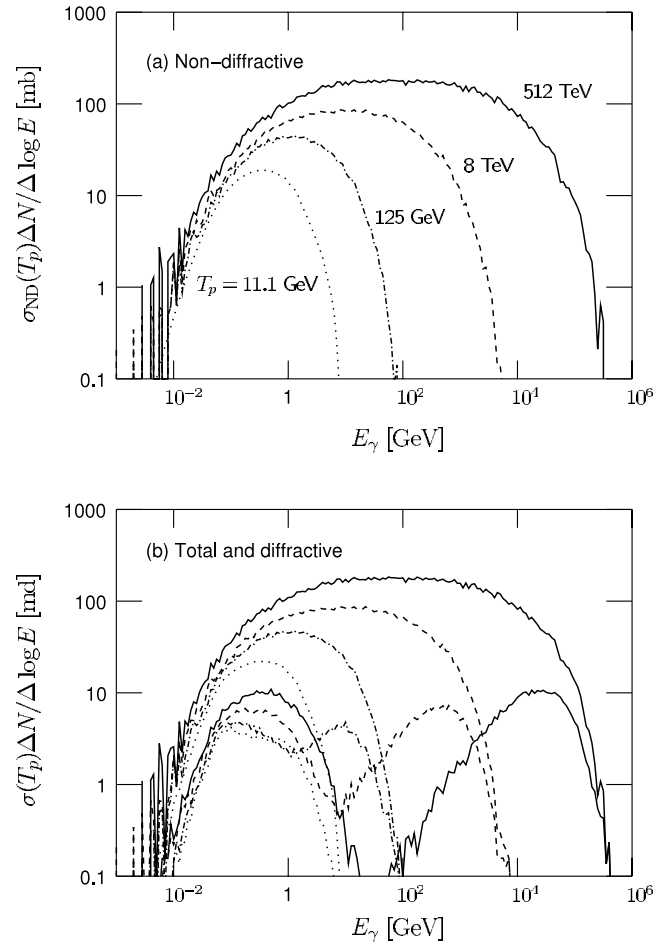


FIG. 7.—Gamma-ray inclusive cross sections by readjusted model A for four monoenergetic protons for (a) the nondiffractive process and (b) the total (top four curves) and the diffractive process (bottom four curves). Note that the diffractive process produces two humps at  $T_p = 512$  TeV, 8 TeV, and 125 GeV. The four proton kinetic energies are  $T_p = 512$  TeV (solid line), 8 TeV (dashed line), 125 GeV (dot-dashed line), and 11.1 GeV (dotted line). The bin width is  $\Delta \log E = 0.05$ . The large fluctuation in the curves at the highest and lowest ends are due to statistics in the simulation.

around  $1600 \text{ MeV}/c^2$ : its pion multiplicities ( $+$ : $0$ : $-$ ) are assumed to be  $1.0 : 0.8 : 0.2$ . We note here that the resonance components significantly favor positive pions over neutral pions while negative pions are strongly suppressed.

The distribution of pion kinetic energy in the  $p$ - $p$  center-of-mass (CM) system ( $T_\pi$ ) has been adjusted to reproduce the experimental ones given in Figures 3–5 of Dermer (1986a). For the  $\Delta(1232)$  excitation, the probability increases proportionally to  $T_\pi$  up to its maximum, set at  $T_\pi = 0.28 \text{ abs}(T_p - 0.4)^{0.45}$ . Here  $T_\pi$  and  $T_p$  are measured in  $\text{GeV}/c$ . The distribution goes to zero beyond this maximum value. For  $\text{res}(1600)$ , the probability increases proportionally to  $T_\pi$  to reach its peak at  $T_\pi = 0.16 \text{ abs}(T_p - 0.4)^{0.45}$ . It decreases linearly until reaching zero at twice the peak of  $T_\pi$ .

Pion momentum is directed isotropically in the  $p$ - $p$  CM system for  $\text{res}(1600)$  as well as for  $\Delta(1232)$ . No angular correlation has been assumed between the two pions from  $\text{res}(1600)$ : this is justified for the astronomical environment, where the chance of detecting two gamma rays from a same interaction is null. Decay kinematics including the polarization effect has been implemented to the charged pion decay. This treatment allows the resonances to recoil transversely to the direction of the incident proton while the

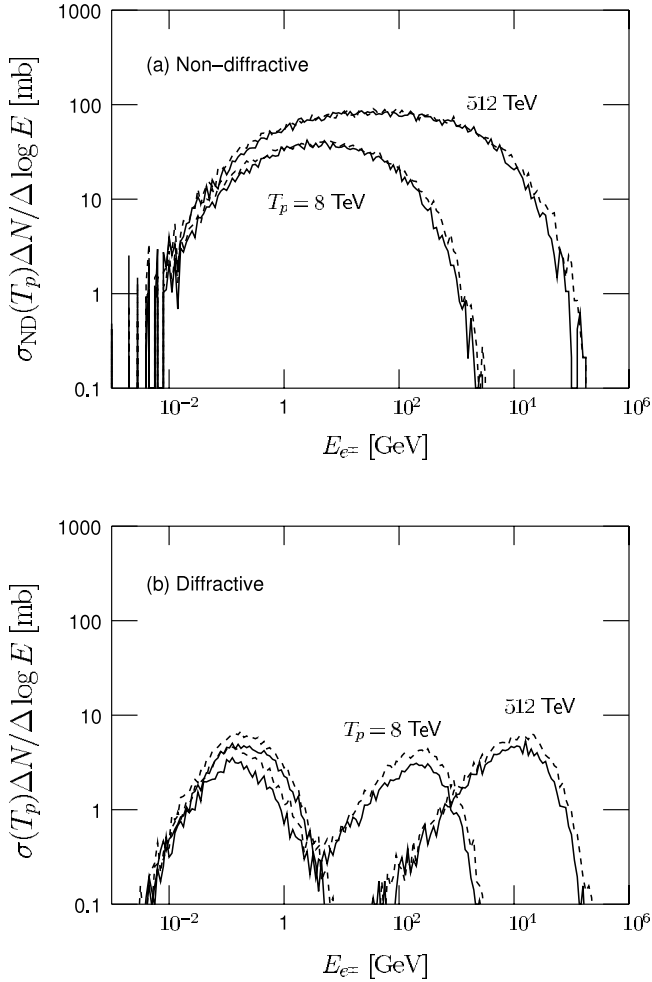


FIG. 8.—Electron and positron inclusive cross sections by readjusted model A for  $T_p = 8$  and 512 TeV for (a) the nondiffractive and (b) diffractive processes. Electron spectra are shown by solid lines and positron spectra by dashed lines. Note that the spectra have two humps in the diffractive process. The bin width is  $\Delta \log E = 0.05$ . The large fluctuation in the histograms at the highest and lowest ends are due to statistics in the simulation.

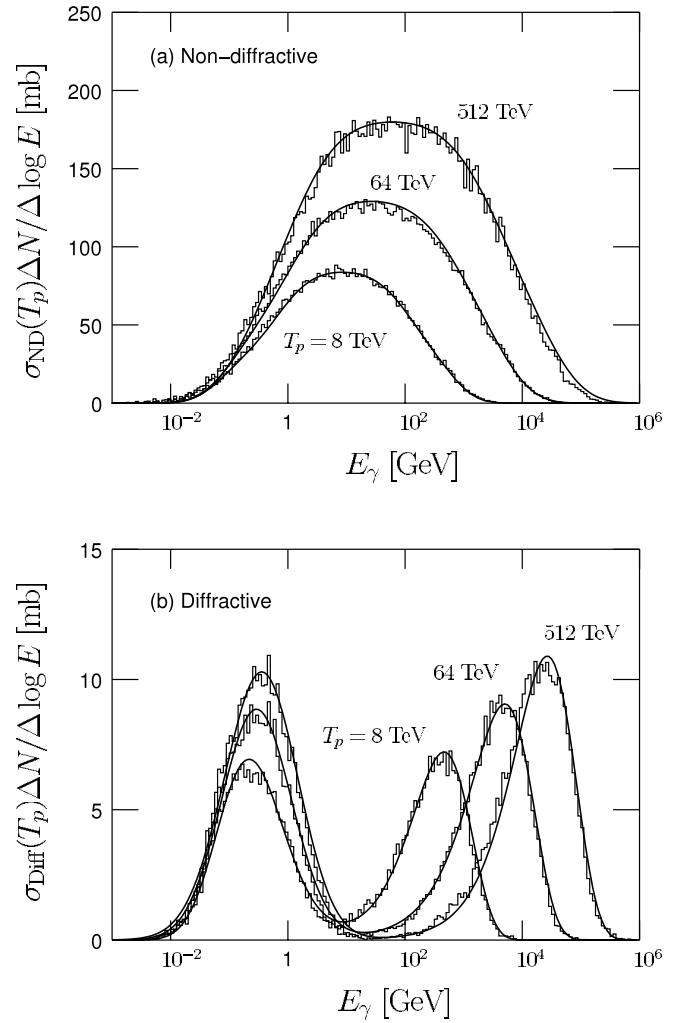


FIG. 9.—Simulated (*histograms*) and parameterized (*solid lines*) gamma-ray inclusive cross sections for (a) nondiffractive and (b) diffractive processes for  $T_p = 8, 64,$  and 512 TeV. The parameterized cross sections are defined by equations (6) and (9), and parameters given in Table 3.

recoil was constrained along the incident proton direction in Stecker (1970).

To validate the resonance components of the readjusted model A, we have compared the model  $\pi^0$  spectrum in the  $p$ - $p$  CM system at  $T_p = 0.65, 0.97,$  and 2.0 GeV with experimental data in Figures 3, 4, and 5. Shown in these figures are contributions of the  $\Delta(1232), \text{res}(1600),$  nondiffractive, and diffractive processes. Our model reproduces well the shape of pion kinetic energy distribution at  $T_p = 0.65$  GeV but begins to concentrate more toward zero kinetic energy than experimental data at  $T_p = 0.97$  and 2.0 GeV. Fidelity to the experimental data is much improved

TABLE 2  
KINEMATIC LIMIT PARAMETERS FOR THE NONDIFFRACTIVE PROCESS

Particle	$L_{\max}$	$W_{\text{ND},l}$	$W_{\text{ND},h}$
$\gamma$ .....	$0.96 \log T_p$	15	44
$e^-$ .....	$0.96 \log T_p$	20	45
$e^+$ .....	$0.94 \log T_p$	15	47
$\nu_e$ .....	$0.98 \log T_p$	15	42
$\bar{\nu}_e$ .....	$0.98 \log T_p$	15	40
$\nu_\mu$ .....	$0.94 \log T_p$	20	45
$\bar{\nu}_\mu$ .....	$0.98 \log T_p$	15	40

NOTE.—Proton kinetic energy  $T_p$  is in GeV.

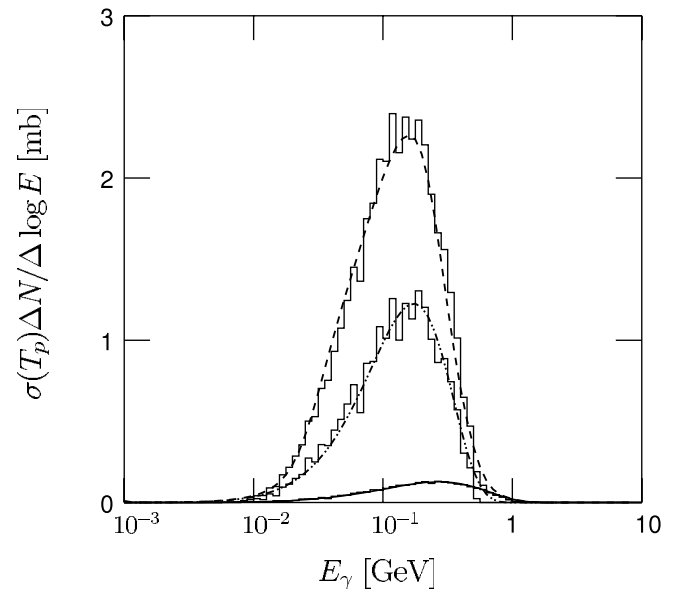


FIG. 10.—Simulated (*histograms*) and parameterized (*lines*) gamma-ray inclusive cross sections for the resonance-excitation processes at  $T_p = 0.69$  GeV.  $\Delta(1232)$  (*double-dot-dashed line*),  $\text{res}(1600)$  (*thin solid line*), and the sum of all model distributions (*dashed line*). The parameterized cross sections are defined by equations (12) for both  $\Delta(1232)$  and  $\text{res}(1600)$ , and parameters are given in Table 3.

TABLE 3  
PARAMETERS DESCRIBING GAMMA-RAY SPECTRA FOR ARBITRARY PROTON ENERGY

Parameter	Formulae as Functions of the Proton Kinetic Energy ( $y = \log T_p$ ) in TeV
Nondiffraction, eq. (6)	
$a_0$ .....	$-0.51187(y + 3.3) + 7.6179(y + 3.3)^2 - 2.1332(y + 3.3)^3 + 0.22184(y + 3.3)^4$
$a_1$ .....	$-(1.2592 \times 10^{-5}) + (1.4439 \times 10^{-5}) \exp(-0.29360(y + 3.4)) + (5.9363 \times 10^{-5})/(y + 4.1485) + (2.2640 \times 10^{-6})y - (3.3723 \times 10^{-7})y^2$
$a_2$ .....	$-(174.83 + 152.78) \log [1.5682(y + 3.4)] - 808.74/(y + 4.6157)$
$a_3$ .....	$0.81177 + 0.56385y + 0.0040031y^2 - 0.0057658y^3 + 0.00012057y^4$
$a_4$ .....	$0.68631(y + 3.32) + 10.145(y + 3.32)^2 - 4.6176(y + 3.32)^3 + 0.86824(y + 3.32)^4 - 0.053741(y + 3.32)^5$
$a_5$ .....	$+(9.0466 \times 10^{-7}) + (1.4539 \times 10^{-6}) \log [0.015204(y + 3.4)] + (1.3253 \times 10^{-4})/(y + 4.7171)^2 - (4.1228 \times 10^{-7})y + (2.2036 \times 10^{-7})y^2$
$a_6$ .....	$-(339.45 + 618.73) \log [0.31595(y + 3.9)] + 250.20/(y + 4.4395)^2$
$a_7$ .....	$-35.105 + 36.167y - 9.3575y^2 + 0.33717y^3$
$a_8$ .....	$0.17554 + 0.37300y - 0.014938y^2 + 0.0032314y^3 + 0.0025579y^4$
$r(y)$ .....	$3.05 \exp(-107\{(y + 3.25)/[1 + 8.08(y + 3.25)]\}^2)$ for $T_p \leq 1.95$ GeV, 1.01 for $T_p > 1.95$ GeV
Diffraction, eq. (9) <sup>a</sup>	
$b_0$ .....	$60.142 \tanh[-0.37555(y + 2.2)] - 5.9564(y + 0.59913)^2 + 6.0162 \times 10^{-3}(y + 9.4773)^4$
$b_1$ .....	$35.322 + 3.8026 \tanh[-2.5979(y + 1.9)] - 2.1870 \times 10^{-4}(y + 369.13)^2$
$b_2$ .....	$-15.732 - 0.082064 \tanh[-1.9621(y + 2.1)] + 2.3355 \times 10^{-4}(y + 252.43)^2$
$b_3$ .....	$-0.086827 + 0.37646 \exp(-0.53053\{(y + 1.0444)/[1.0 + 0.27437(y + 1.0444)]\}^2)$
$b_4$ .....	$2.5982 + 0.39131(y + 2.95)^2 - 0.0049693(y + 2.95)^4 + 0.94131 \exp(-24.347[y + 2.45 - 0.19717(y + 2.45)^2]^2)$
$b_5$ .....	$0.11198 - 0.64582y + 0.16114y^2 + 2.2853 \exp(-0.0032432\{(y - 0.83562)/[1.0 + 0.33933(y - 0.83562)]\}^2)$
$b_6$ .....	$1.7843 + 0.91914y + 0.050118y^2 + 0.038096y^3 - 0.027334y^4 - 0.0035556y^5 + 0.0025742y^6$
$b_7$ .....	$-0.19870 - 0.071003y + 0.019328y^2 - 0.28321 \times \exp(-6.0516(y + 1.8441)^2)$
$\Delta(1232)$ , eq. (12)	
$c_0$ .....	$2.4316 \exp(-69.484\{(y + 3.1301)/[1.0 + 1.24921(y + 3.1301)]\}^2) - 6.3003 - 9.5349/y + 0.38121y^2$
$c_1$ .....	$56.872 + 40.627y + 7.7528y^2$
$c_2$ .....	$-5.4918 - 6.7872 \tanh[4.7128(y + 2.1)] + 0.68048y$
$c_3$ .....	$-0.36414 + 0.039777y$
$c_4$ .....	$-0.72807 - 0.48828y - 0.092876y^2$
res(1600), eq. (12) <sup>b</sup>	
$d_0$ .....	$3.2433 \exp(-57.133\{(y + 2.9507)/[1.0 + 1.2912(y + 2.9507)]\}^2) - 1.0640 - 0.43925y$
$d_1$ .....	$16.901 + 5.9539y - 2.1257y^2 - 0.92057y^3$
$d_2$ .....	$-6.6638 - 7.5010 \tanh[30.322(y + 2.1)] + 0.54662y$
$d_3$ .....	$-1.50648 - 0.87211y - 0.17097y^2$
$d_4$ .....	$0.42795 + 0.55136y + 0.20707y^2 + 0.027552y^3$

<sup>a</sup>  $b_0, \dots, b_3 = 0$  for  $T_p < 5.52$  GeV

<sup>b</sup> Parameters  $c_0, \dots, c_4$  replaced with  $d_0, \dots, d_4$ .

when compared with the model by Stephens & Badhwar (1981) but somewhat worse than the one by Stecker (1970) given in Figures 2–6 of Dermer (1986a). The difference among the models becomes less noticeable for pion decay products, gamma rays, electrons, positrons, and neutrinos.

Our inclusive  $\pi^0$  cross section, the sum of all four components, is compared with experimental data assembled by Stecker (1970) and Dermer (1986a) in Figure 6. The readjusted model A reproduces experimental data quite well for a wide range of incident proton energy.

#### 4. INCLUSIVE SPECTRA OF SIMULATED EVENTS FOR MONOENERGETIC PROTON BEAM

The first step of parameterization is to generate simulated events for monoenergetic protons. To simplify this step, events have been generated for discrete proton energies at a geometrical series of  $T_p = 1000.0 \times 2^{(N-22)/2}$  GeV, where  $N = 0-40$ . Each proton kinetic energy ( $T_p$ ) represents a bin covering between  $2^{-0.25}T_p$  and  $2^{0.25}T_p$ . The sampling density has been increased for  $T_p < 1$  GeV by adding points at  $T_p = 0.58$  and  $0.82$  GeV.

Secondary particle spectra are histogrammed from these simulated events in energy bins of width  $\Delta E/E = 5\%$ . Figures 7a and 7b show thus-obtained inclusive gamma-ray cross sections for the nondiffractive and diffractive processes, for  $T_p = 512$  TeV, 8 TeV, 125 GeV, and 11.1 GeV, respectively. Those for  $e^\pm$  are given in Figures 8 and 512 TeV in Figures 8a and 8b.

We then define, after several iterations of fitting, functional formulae that reproduce the secondary particle spectra for monoenergetic protons for the nondiffractive, diffractive, and resonance-excitation processes separately. For the nondiffractive process, the differential inclusive cross section ( $\Delta\sigma_{\text{ND}}$ ) to produce a secondary particle in a bin of width  $\Delta E_{\text{sec}}/E_{\text{sec}} = 100\%$  centered at  $E_{\text{sec}}$  is given as

$$\frac{\Delta\sigma_{\text{ND}}(E_{\text{sec}})}{\Delta \log(E_{\text{sec}})} = F_{\text{ND}}(x)F_{\text{ND,kl}}(x), \quad (5)$$

where  $E_{\text{sec}}[\text{GeV}]$  is the energy of the secondary particle and  $x = \log(E_{\text{sec}}[\text{GeV}])$ ,  $F_{\text{ND}}(x)$  is the formula representing the nondiffractive cross section, given in equation (6) below, and  $F_{\text{ND,kl}}(x)$

is the formula to approximately enforce the energy-momentum conservation limits:

$$F_{\text{ND}}(x) = a_0 \exp\left\{-a_1 [x - a_3 + a_2(x - a_3)^2]^2\right\} + a_4 \exp\left\{-a_5 [x - a_8 + a_6(x - a_8)^2 + a_7(x - a_8)^3]^2\right\}, \quad (6)$$

$$F_{\text{ND,kl}}(x) = \frac{1}{\exp[W_{\text{ND,l}}(L_{\text{min}} - x)] + 1} \times \frac{1}{\exp[W_{\text{ND,h}}(x - L_{\text{max}})] + 1}, \quad (7)$$

where  $L_{\text{min}}$  and  $L_{\text{max}}$  are the lower and upper kinematic limits imposed and  $W_{\text{ND,l}}$  and  $W_{\text{ND,h}}$  are the widths of the kinematic cutoffs;  $L_{\text{min}} = -2.6$  for all secondary particles, and the other parameters are listed in Table 2.

For the diffractive process we use a similar function

$$\frac{\Delta\sigma_{\text{diff}} E_{\text{sec}}}{\Delta \log E_{\text{sec}}} = F_{\text{Diff}}(x) F_{\text{kl}}(x), \quad (8)$$

where  $E_{\text{sec}}$  [GeV] is the energy of the secondary particle and  $x = \log(E_{\text{sec}}[\text{GeV}])$ ;  $F_{\text{diff}}(x)$  represents the diffractive cross section, given in equation (9) below, and  $F_{\text{kl}}(x)$  enforces the energy-momentum conservation:

$$F_{\text{diff}}(x) = b_0 \exp\left\{-b_1 \left\{\frac{x - b_2}{1 + b_3(x - b_2)}\right\}^2\right\} + b_4 \exp\left\{-b_5 \left\{\frac{x - b_6}{1 + b_7(x - b_6)}\right\}^2\right\}, \quad (9)$$

$$F_{\text{kl}}(x) = \frac{1}{\exp[W_{\text{diff}}(x - L_{\text{max}})] + 1}, \quad (10)$$

with  $W_{\text{diff}} = 75$  and  $L_{\text{max}} = \log(T_p[\text{GeV}])$ .

For the resonance-excitation processes [ $\Delta(1232)$  and  $\text{res}(1600)$ ] we use the function

$$\frac{\Delta\sigma_{\text{res}}(E_{\text{sec}})}{\Delta \log(E_{\text{sec}})} = F_{\text{res}}(x) F_{\text{kl}}(x), \quad (11)$$

where  $E_{\text{sec}}$  [GeV] is the energy of the secondary particle and  $x = \log(E_{\text{sec}}[\text{GeV}])$ ,  $F_{\text{res}}(x)$  represents the cross section, given in equation (12) below, and  $F_{\text{kl}}(x)$ , which is the same as for the diffraction process, enforces the energy-momentum conservation:

$$F_{\text{res}}(x) = c_0 \exp\left\{-c_1 \left\{\frac{x - c_2}{1 + c_3(x - c_2) + c_4(x - c_2)^2}\right\}^2\right\}. \quad (12)$$

To ensure that the parameterized model reproduces the experimental  $\pi^0$  multiplicity after the readjustment in the resonance-excitation region of  $T_p$ , we have renormalized the nondiffractive contribution by multiplying it with a renormalization factor,  $r(T_p)$ , given below, to the final spectrum. Note that this readjustment does not affect the diffractive process:

$$r(T_p) \simeq 1.01 \text{ for } T_p > 1.95 \text{ GeV}, \quad (13)$$

$$r(y = \log T_p) = 3.05 \exp\left\{-107 \left\{\frac{y + 3.25}{1 + 8.08(y + 3.25)}\right\}^2\right\} \text{ for } T_p \leq 1.95 \text{ GeV}. \quad (14)$$

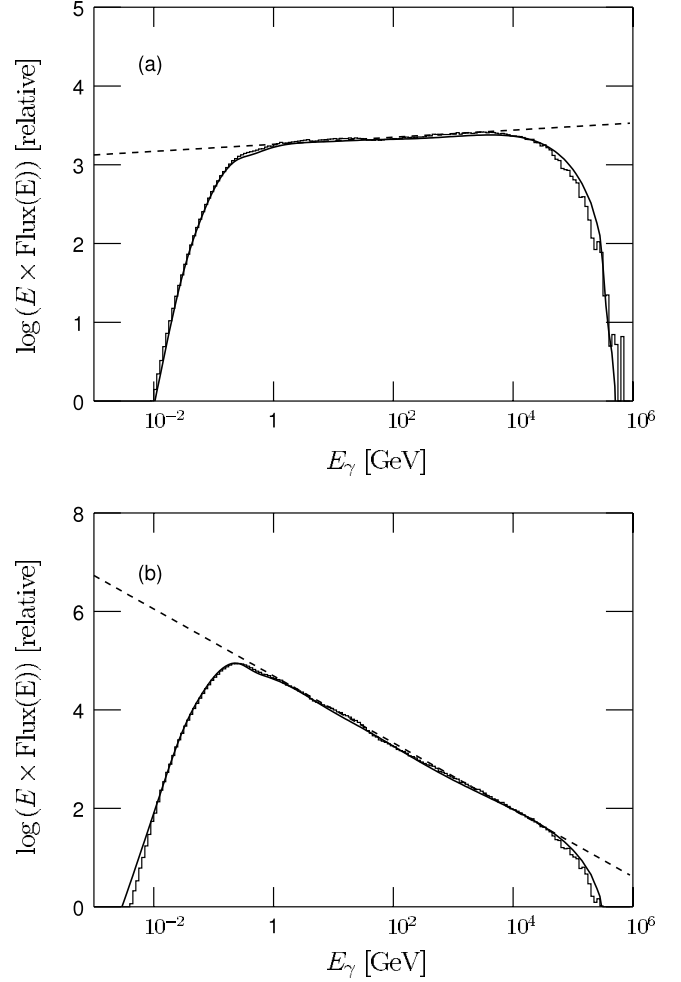


FIG. 11.—Gamma-ray spectra produced by protons with power-law spectrum cutoff at  $T_p = 512$  TeV: (a) index = 2 and (b) index = 2.7 by the parameterized model (solid lines) defined by equations (6), (9), and (12), and by Table 3. The histograms are those of the simulation by the readjusted model A. The dashed straight line corresponds to an index of (a) 1.95 and (b) 2.68.

For all other secondary particles,  $r(y = \log T_p)$  is found in Tables 4–9.

The simulated gamma-ray inclusive cross sections are superimposed with the parameterized ones in Figures 9a and 9b for three monoenergetic protons, for the nondiffractive and diffractive processes, and for the resonance-excitation processes in Figure 10. The agreement is generally good except near the higher and lower kinematical limits, where we find a difference of about 10%–20%.

## 5. REPRESENTATION OF PARAMETERS AS FUNCTIONS OF INCIDENT PROTON ENERGY

The parameterization formulae for secondary particles for monoenergetic protons (eqs. [6], [9], and [12]) have nine, eight, and five parameters for each  $T_p$  for nondiffractive, diffractive, and resonance-excitation processes, respectively. These parameters depend on the proton kinetic energy,  $T_p$ . The final step of the parameterization is to find simple functions representing energy dependence of these parameters. Functions obtained by fitting often give values significantly different from those found for monoenergetic protons near the kinematic limits and produce artifacts in the wide range spectral energy density, as described previously. Some manual adjustments have been made to control possible artifacts.

TABLE 4  
PARAMETERS DESCRIBING ELECTRON SPECTRA FOR ARBITRARY PROTON ENERGY

Parameter	Formulae as Functions of the Proton Kinetic Energy ( $y = \log T_p$ ) in TeV.
Nondiffraction, eq. (6)	
$a_0$ .....	$-0.018639(y + 3.3) + 2.4315(y + 3.3)^2 - 0.57719(y + 3.3)^3 + 0.063435(y + 3.3)^4$
$a_1$ .....	$(7.1827 \times 10^{-6}) - (3.5067 \times 10^{-6})y + (1.3264 \times 10^{-6})y^2 - (3.3481 \times 10^{-7})y^3 + (2.3551 \times 10^{-8})y^4 + (3.4297 \times 10^{-8})y^5$
$a_2$ .....	$563.91 - 362.18 \log [2.7187(y + 3.4)] - (2.8924 \times 10^4)/(y + 7.9031)^2$
$a_3$ .....	$0.52684 + 0.57717y + 0.0045336y^2 - 0.0089066y^3$
$a_4$ .....	$0.36108(y + 3.32) + 1.6963(y + 3.32)^2 - 0.074456(y + 3.32)^3 - 0.071455(y + 3.32)^4 + 0.010473(y + 3.32)^5$
$a_5$ .....	$(9.7387 \times 10^{-5}) + (7.8573 \times 10^{-5}) \log [0.0036055(y + 4.3)] + 0.00024660/(y + 4.9390) - (3.8097 \times 10^{-7})y^2$
$a_6$ .....	$-273.00 - 106.22 \log [0.34100(y + 3.4)] + 89.037y - 12.546y^2$
$a_7$ .....	$432.53 - 883.99 \log [0.19737(y + 3.9)] - (4.1938 \times 10^4)/(y + 8.5518)^2$
$a_8$ .....	$-0.12756 + 0.43478y - 0.0027797y^2 - 0.0083074y^3$
$r(y)$ .....	$3.63 \exp(-106\{(y + 3.26)/[1 + 9.21(y + 3.26)]\}^2) - 0.182y - 0.175y^2$ for $T_p \leq 15.6$ GeV, 1.01 for $T_p > 15.6$ GeV
Diffraction, eq. (9) <sup>a</sup>	
$b_0$ .....	$0.20463 \tanh [-6.2370(y + 2.2)] - 0.16362(y + 1.6878)^2 + 3.5183 \times 10^{-4}(y + 9.6400)^4$
$b_1$ .....	$1.6537 + 3.8530 \exp(-3.2027\{(y + 2.0154)/[1.0 + 0.62779(y + 2.0154)]\}^2)$
$b_2$ .....	$-10.722 - 0.082672 \tanh [-1.8879(y + 2.1)] + 1.4895 \times 10^{-4}(y + 256.63)^2$
$b_3$ .....	$-0.023752 - 0.51734 \exp(-3.3087\{(y + 1.9877)/[1.0 + 0.40300(y + 1.9877)]\}^2)$
$b_4$ .....	$0.94921 + 0.12280(y + 2.9)^2 - 7.1585 \times 10^{-4}(y + 2.9)^4 + 0.52130 \log(y + 2.9)$
$b_5$ .....	$-4.2295 - 1.0025 \tanh [9.0733(y + 1.9)] - 0.11452 \times (y - 62.382)$
$b_6$ .....	$1.4862 + 0.99544y - 0.042763y^2 - 0.0040065y^3 + 0.0057987y^4$
$b_7$ .....	$6.2629 + 6.9517 \tanh [-0.36480(y + 2.1)] - 0.026033 \times (y - 2.8542)$
res(1600), eq. (12) <sup>b</sup>	
$d_0$ .....	$0.37790 \exp(-56.826\{(y + 2.9537)/[1.0 + 1.5221(y + 2.9537)]\}^2) - 0.059458 + 0.0096583y^2$
$d_1$ .....	$-5.5135 - 3.3988y$
$d_2$ .....	$-7.1209 - 7.1850 \tanh [30.801(y + 2.1)] + 0.35108y$
$d_3$ .....	$-6.7841 - 4.8385y - 0.91523y^2$
$d_4$ .....	$-134.03 - 139.63y - 48.316y^2 - 5.5526y^3$

<sup>a</sup>  $b_0, \dots, b_3 = 0$  for  $T_p < 5.52$  GeV.

<sup>b</sup> Parameters  $c_0, \dots, c_4$  replaced with  $d_0, \dots, d_4$ .

TABLE 5  
PARAMETERS DESCRIBING POSITRON SPECTRA FOR ARBITRARY PROTON ENERGY

Parameters	Formulae as Functions of the Proton Kinetic Energy ( $y = \log T_p$ ) in TeV.
Nondiffraction, eq. (6)	
$a_0$ .....	$-0.79606(y + 3.3) + 7.7496(y + 3.3)^2 - 3.9326(y + 3.3)^3 + 0.80202(y + 3.3)^4 - 0.054994(y + 3.3)^5$
$a_1$ .....	$(6.7943 \times 10^{-6}) - (3.5345 \times 10^{-6})y + (6.0927 \times 10^{-7})y^2 + (2.0219 \times 10^{-7})y^3 + (5.1005 \times 10^{-8})y^4 - (4.2622 \times 10^{-8})y^5$
$a_2$ .....	$44.827 - 81.378 \log [0.027733(y + 3.5)] - (1.3886 \times 10^4)/(y + 8.4417)$
$a_3$ .....	$0.52010 + 0.59336y + 0.012032y^2 - 0.0064242y^3$
$a_4$ .....	$2.1361(y + 3.32) + 1.8514(y + 3.32)^2 - 0.47872(y + 3.32)^3 + 0.0032043(y + 3.32)^4 + 0.0082955(y + 3.32)^5$
$a_5$ .....	$(1.0845 \times 10^{-6}) + (1.4336 \times 10^{-6}) \log [0.0077255(y + 4.3)] + (1.3018 \times 10^{-4})/(y + 4.8188)^2 + (9.3601 \times 10^{-8})y$
$a_6$ .....	$-267.74 + 14.175 \log [0.35391(y + 3.4)] + 64.669/(y - 7.7036)^2$
$a_7$ .....	$138.26 - 539.84 \log [0.12467(y + 3.9)] - (1.9869 \times 10^4)/(y + 7.6884)^2 + 1.0675y^2$
$a_8$ .....	$-0.14707 + 0.40135y + 0.0039899y^2 - 0.0016602y^3$
$r(y)$ .....	$2.22 \exp(-98.9\{(y + 3.25)/[1 + 10.4(y + 3.25)]\}^2)$ for $T_p \leq 5.52$ GeV, 1.0 for $T_p > 5.52$ GeV
Diffraction, eq. (9) <sup>a</sup>	
$b_0$ .....	$29.192 \tanh [-0.37879(y + 2.2)] - 3.2196(y + 0.67500)^2 + 0.0036687(y + 9.0824)^4$
$b_1$ .....	$-142.97 + 147.86 \exp(-0.37194\{(y + 1.8781)/[1.0 + 3.8389(y + 1.8781)]\}^2)$
$b_2$ .....	$-14.487 - 4.2223 \tanh [-13.546(y + 2.2)] + 1.6988 \times 10^{-4}(y + 234.65)^2$
$b_3$ .....	$-0.0036974 - 0.41976 \exp(-6.1527\{(y + 1.8194)/[1.0 + 0.99946(y + 1.8194)]\}^2)$
$b_4$ .....	$1.8108 + 0.18545(y + 2.9)^2 - 0.0020049(y + 2.9)^4 + 0.85084 \exp\{-14.987[x + 2.29 - 0.18967(x + 2.29)^2]^2\}$
$b_5$ .....	$2.0404 - 0.51548 \tanh [2.2758(y + 1.9)] - 0.035009/(y - 6.6555)$
$b_6$ .....	$1.5258 + 1.0132y - 0.064388y^2 - 0.0040209y^3 - 0.0082772y^4$
$b_7$ .....	$3.0551 + 3.5240 \tanh [-0.36739(y + 2.1)] - 0.13382 \times (y - 2.7718)$
$\Delta(1232)$ , eq. (12)	
$c_0$ .....	$2.9841 \exp(-67.857\{(y + 3.1272)/[1.0 + 0.22831(y + 3.1272)]\}^2) - 6.5855 - 9.6984/y + 0.41256y^2$
$c_1$ .....	$6.8276 + 5.2236y + 1.4630y^2$
$c_2$ .....	$-6.0291 - 6.4581 \tanh [5.0830(y + 2.1)] + 0.46352y$
$c_3$ .....	$0.59300 + 0.36093y$
$c_4$ .....	$0.77368 + 0.44776y + 0.056409y^2$
res(1600), eq. (12) <sup>b</sup>	
$d_0$ .....	$1.9186 \exp(-56.544\{(y + 2.9485)/[1.0 + 1.2892(y + 2.9485)]\}^2) - 0.23720 + 0.041315y^2$
$d_1$ .....	$-4.9866 - 3.1435y$
$d_2$ .....	$-7.0550 - 7.2165 \tanh [31.033(y + 2.1)] + 0.38541y$
$d_3$ .....	$-2.8915 - 2.1495y - 0.45006y^2$
$d_4$ .....	$-1.2970 - 0.13947y - 0.41197y^2 - 0.10641y^3$

<sup>a</sup>  $b_0, \dots, b_3 = 0$  for  $T_p < 11.05$  GeV.

<sup>b</sup> Parameters  $c_0, \dots, c_4$  replaced with  $d_0, \dots, d_4$ .

TABLE 6  
PARAMETERS DESCRIBING ELECTRON NEUTRINO SPECTRA FOR ARBITRARY PROTON ENERGY

Parameters	Formulae as Functions of the Proton Kinetic Energy ( $y = \log T_p$ ) in TeV
Nondiffraction, eq. (6)	
$a_0$ .....	$0.0074087 + 2.9161(y + 3.31) + 0.99061(y + 3.31)^2 - 0.28694(y + 3.31)^3 + 0.038799(y + 3.31)^4$
$a_1$ .....	$-3.2480 \times 10^{-5} + 7.1944 \times 10^{-5} \exp[-0.21814(y + 3.4)] + 2.0467 \times 10^{-5}/(y + 4.1640) + 5.6954 \times 10^{-6}y - 3.4105 \times 10^{-7}y^2$
$a_2$ .....	$-230.50 + 58.802y - 9.9393y^2 + 1.2473y^3 - 0.26322y^4$
$a_3$ .....	$0.45064 + 0.56930y + 0.012428y^2 - 0.0070889y^3$
$a_4$ .....	$-0.011883 + 1.7992(y + 3.32) + 3.5264(y + 3.32)^2 - 1.7478(y + 3.32)^3 + 0.32077(y + 3.32)^4 - 0.017667(y + 3.32)^5$
$a_5$ .....	$-1.6238 \times 10^{-7} + 1.8116 \times 10^{-6} \exp[-0.30111(y + 3.4)] + 9.6112 \times 10^{-5}/(y + 4.8229)^2$
$a_6$ .....	$-261.30 - 43.351 \log_{10}[0.35298(y + 3.4)] + 70.925/(y - 8.7147)^2$
$a_7$ .....	$184.45 - 1473.6/(y + 6.8788) - 4.0536y^2$
$a_8$ .....	$-0.24019 + 0.38504y + 0.0096869y^2 - 0.0015046y^3$
$r(y)$ .....	$0.329 \exp(-247\{(y + 3.26)/[1 + 6.56(y + 3.26)]\}^2) - 0.957y - 0.229y^2$ for $T_p \leq 7.81$ GeV, 1.0 for $T_p > 7.81$ GeV
Diffraction, eq. (9) <sup>a</sup>	
$b_0$ .....	$53.809 \tanh[-0.41421(y + 2.2)] - 6.7538(y + 0.76010)^2 + 0.0088080(y + 8.5075)^4$
$b_1$ .....	$-50.211 + 55.131 \exp\{1.3651((y + 1.8901)/[1.0 + 4.4440(y + 1.8901)])^2\}$
$b_2$ .....	$-17.231 + 0.041100 \tanh[7.9638(y + 1.9)] - 0.055449y + 2.5866 \times 10^{-4}(y + 250.68)^2$
$b_3$ .....	$12.335 - 12.893 \exp(-1.4412\{(y + 1.8998)/[1.0 + 5.5969(y + 1.8998)]\}^2)$
$b_4$ .....	$1.3558 + 0.46601(y + 2.95) + 0.052978(y + 2.2)^2 + 0.79575 \exp\{-5.4007[y + 2.2 + 4.6121(x + 2.2)]^2\}$
$b_5$ .....	$1.8756 - 0.42169 \tanh[1.6100(y + 1.9)] - 0.051026 \times (y - 3.9573)$
$b_6$ .....	$1.5016 + 1.0118y - 0.072787y^2 - 0.0038858y^3 + 0.0093650y^4$
$b_7$ .....	$4.9735 + 5.5674 \tanh[-0.36249(y + 2.1)] - 0.20660 \times (y - 2.8604)$
$\Delta(1232)$ , eq. (12)	
$c_0$ .....	$2.8290 \exp(-71.339\{(y + 3.1282)/[1.0 + 0.48420(y + 3.1282)]\}^2) - 9.6339 - 15.733/y + 0.52413y^2$
$c_1$ .....	$-24.571 - 15.831y - 2.1200y^2$
$c_2$ .....	$-5.9593 - 6.4695 \tanh[4.7225(y + 2.1)] + 0.50003y$
$c_3$ .....	$0.26022 + 0.24545y$
$c_4$ .....	$0.076498 + 0.061678y + 0.0040028y^2$
res(1600), eq. (12) <sup>b</sup>	
$d_0$ .....	$1.7951 \exp(-57.260\{(y + 2.9509)/[1.0 + 1.4101(y + 2.9509)]\}^2) - 0.58604 - 0.23868y$
$d_1$ .....	$-2.6395 - 1.5105y + 0.22174y^2$
$d_2$ .....	$-7.0512 - 7.1970 \tanh[31.074(y + 2.1)] + 0.39007y$
$d_3$ .....	$-1.4271 - 1.0399y - 0.24179y^2$
$d_4$ .....	$0.74875 + 0.63616y + 0.17396y^2 + 0.017636y^3$

<sup>a</sup>  $b_0, \dots, b_3 = 0$  for  $T_p < 11.05$  GeV

<sup>b</sup> Parameters  $c_0, \dots, c_4$  replaced with  $d_0, \dots, d_4$ .

TABLE 7  
PARAMETERS DESCRIBING ELECTRON ANTINEUTRINO SPECTRA FOR ARBITRARY PROTON ENERGY

Parameters	Formulae as Functions of the Proton Kinetic Energy ( $y = \log T_p$ ) in TeV.
Nondiffraction, eq. (6)	
$a_0$ .....	$0.0013113 + 0.36538(y + 3.31) + 1.5178(y + 3.31)^2 - 0.20668(y + 3.31)^3 + 0.024255(y + 3.31)^4$
$a_1$ .....	$-4.7833 \times 10^{-6} + 4.5837 \times 10^{-5} \exp[-0.42980(y + 3.4)] + 6.1559 \times 10^{-6}/(y + 4.1731) + 1.1928 \times 10^{-6}y$
$a_2$ .....	$-245.22 + 73.223y - 19.652y^2 + 0.083138y^3 + 0.71561y^4$
$a_3$ .....	$0.45232 + 0.52934y + 0.010078y^2 - 0.0017092y^3$
$a_4$ .....	$-0.0025734 + 0.38424(y + 3.32) + 1.5517(y + 3.32)^2 + 0.17336(y + 3.32)^3 - 0.17160(y + 3.32)^4 + 0.021059(y + 3.32)^5$
$a_5$ .....	$4.7673 \times 10^{-5} + 5.4936 \times 10^{-5} \log[0.0067905(y + 4.3)] + 0.00020740/(y + 4.9772)$
$a_6$ .....	$-270.30 - 114.47 \log[0.34352(y + 3.4)] + 80.085y - 7.9240y^2$
$a_7$ .....	$3272.9 - 2.9161 \times 10^5/(y + 87.847) - 6.2330y^2$
$a_8$ .....	$-0.17787 + 0.36771y - 0.025397y^2 + 0.0019238y^3 + 0.0032725y^4$
$r(y)$ .....	$2.67 \exp(-45.7\{(y + 3.27)/[1 + 6.59(y + 3.27)]\}^2) - 0.301y - 0.208y^2$ for $T_p \leq 15.6$ GeV, 1.0 for $T_p > 15.6$ GeV
Diffraction, eq. (9) <sup>a</sup>	
$b_0$ .....	$41.307 \tanh[-0.37411(y + 2.2)] - 4.1223(y + 0.55505)^2 + 0.0042652(y + 9.2685)^4$
$b_1$ .....	$-132.50 + 142.12 \exp(-8.0289\{(y + 1.9196)/[1.0 + 11.530(y + 1.9196)]\}^2)$
$b_2$ .....	$-17.223 + 0.011285 \tanh[-69.746(y + 1.9)] - 0.048233y + 2.5881 \times 10^{-4}(y + 250.77)^2$
$b_3$ .....	$8.1991 - 9.6437 \exp(-45.261\{(y + 1.9292)/[1.0 + 16.682(y + 1.9292)]\}^2)$
$b_4$ .....	$0.55919 + 0.36647(y + 2.95)^2 + 0.056194(y + 2.95)^4 + 0.49957 \exp\{-5.5317[y + 2.2 + 0.43867(y + 2.2)]^2\}$
$b_5$ .....	$1.2544 - 0.52362 \tanh[2.7638(y + 1.9)] + 0.055837 \times (y - 17.638)$
$b_6$ .....	$1.4788 + 1.0278y - 0.092852y^2 - 0.0062734y^3 + 0.011920y^4$
$b_7$ .....	$5.1651 + 5.7398 \tanh[-0.37356(y + 2.1)] - 0.22234 \times (y - 2.7889)$
res(1600), eq. (12) <sup>b</sup>	
$d_0$ .....	$0.36459 \exp(-58.210\{(y + 2.9537)/[1.0 + 1.4320(y + 2.9537)]\}^2) - 0.11283 - 0.046244y$
$d_1$ .....	$-9.5066 - 5.4655y - 0.31769y^2$
$d_2$ .....	$-7.1831 - 7.1551 \tanh[30.354(y + 2.1)] + 0.33757y$
$d_3$ .....	$2.7938 + 1.6992y + 0.20161y$
$d_4$ .....	$0.61878 + 0.62371y + 0.18913y^2 + 0.019118y^3$

<sup>a</sup>  $b_0, \dots, b_3 = 0$  for  $T_p < 11.05$  GeV

<sup>b</sup> Parameters  $c_0, \dots, c_4$  replaced with  $d_0, \dots, d_4$ .

TABLE 8  
PARAMETERS DESCRIBING MUON NEUTRINO SPECTRA FOR ARBITRARY PROTON ENERGY

Parameters	Formulae as Functions of the Proton Kinetic Energy ( $y = \log T_p$ ) in TeV.
Nondiffraction, eq. (6)	
$a_0$ .....	$-0.63611(y + 3.3) + 9.9015(y + 3.3)^2 - 4.5897(y + 3.3)^3 + 0.91778(y + 3.3)^4 - 0.060724(y + 3.3)^4$
$a_1$ .....	$6.8700 \times 10^{-6} - 2.8245 \times 10^{-6}y + 7.6032 \times 10^{-7}y^2 - 3.2953 \times 10^{-7}y^3 + 7.4292 \times 10^{-8}y^4$
$a_2$ .....	$-240.46 + 58.405y - 9.8556y^2 + 3.1401y^3 - 0.88932y^4$
$a_3$ .....	$0.49935 + 0.60919y + 0.0024963y^2 - 0.0099910y^3$
$a_4$ .....	$2.5094(y + 3.32) + 4.1350(y + 3.32)^2 - 0.89534(y + 3.32)^3 - 0.0027577(y + 3.32)^4 + 0.014511(y + 3.32)^5$
$a_5$ .....	$8.2046 \times 10^{-7} + 1.4085 \times 10^{-6} \log [0.016793(y + 4.3)] + 0.00013340/(y + 4.7136)^2$
$a_6$ .....	$-267.55 - 0.21018 \log_{10}[0.35217(y + 3.9)] + 69.586y - 9.9930y^2$
$a_7$ .....	$2742.8 + 222.01 \log [9.7401(y + 3.9)] - 4772.5/(y + 19.773) - 6.1001y^2$
$a_8$ .....	$-0.11857 + 0.39072y - 0.037813y^2 + 0.0022265y^3 + 0.0046931y^4$
$r(y)$ .....	$2.23 \exp(-93.4\{(y + 3.25)/[1 + 8.38(y + 3.25)]\}^2) - 0.376y - 0.121y^2$ for $T_p \leq 15.6$ GeV, 1.0 for $T_p > 15.6$ GeV
Diffraction, eq. (9) <sup>a</sup>	
$b_0$ .....	$64.682 \tanh [-0.34313(y + 2.2)] - 5.5955(y + 0.44754)^2 + 0.0050117(y + 9.9165)^4$
$b_1$ .....	$-7.6016 + 3.0427 \times 10^4 \exp(-1.0134 \times 10^4((y + 2.3066)/[1.0 + 41.612(y + 2.3066)])^2)$
$b_2$ .....	$-1.4978 - 0.58163 \tanh [-0.36488(y + 1.9)] + 0.031825(y + 2.8097) + 0.022796(y - 1.8861)^2$
$b_3$ .....	$-0.0061483 - 65.799 \exp(-4.8239\{(y + 3.8835)/[1.0 + 0.53343(y + 3.8835)]\}^2)$
$b_4$ .....	$2.8009 + 0.35341(y + 2.95)^2 - 0.0039779(y + 2.95)^4 + 1.3012 \exp\{-10.592[y + 2.2 - 0.19149(y + 2.2)^2]^2\}$
$b_5$ .....	$1.8016 - 0.69847 \tanh [2.8627(y + 1.9)] - 0.015722 \times (y - 45.4)$
$b_6$ .....	$1.4617 + 1.0167y - 0.078617y^2 - 0.0038336y^3 + 0.010141y^4$
$b_7$ .....	$3.5599 + 4.0041 \tanh [-0.41889(y + 2.1)] - 0.18182 \times (y - 2.4209)$
$\Delta(1232)$ , eq. (12)	
$c_0$ .....	$3.6052 \exp(-60.914\{(y + 3.1278)/[1.0 - 0.19497(y + 3.1278)]\}^2) - 0.92514 + 2.1315/y + 0.23548y^2$
$c_1$ .....	$95.310 + 70.497y + 13.636y^2$
$c_2$ .....	$-6.2158 - 6.2939 \tanh [21.592(y + 2.1)] + 0.37440y$
$c_3$ .....	$2.7485 + 1.1692y$
$c_4$ .....	$-2.7568 - 1.8461y - 0.31376y^2$
res(1600), eq. (12) <sup>b</sup>	
$d_0$ .....	$2.5489 \exp(-58.488\{(y + 2.9509)/[1.0 + 1.3154(y + 2.9509)]\}^2) - 0.83039 - 0.34412y$
$d_1$ .....	$88.173 + 65.148y + 12.585y^2$
$d_2$ .....	$-7.0962 - 7.1690 \tanh [30.890(y + 2.1)] + 0.38032y$
$d_3$ .....	$-4.1440 - 3.2717y - 0.70537y^2$
$d_4$ .....	$2.2624 + 1.1806y - 0.0043450y^2 - 0.043020y^3$

<sup>a</sup>  $b_0, \dots, b_3 = 0$  for  $T_p < 11.05$  GeV.

<sup>b</sup> Parameters  $c_0, \dots, c_4$  replaced with  $d_0, \dots, d_4$ .

TABLE 9  
PARAMETERS DESCRIBING MUON ANTINEUTRINO SPECTRA FOR ARBITRARY PROTON ENERGY

Parameters	Formulae as Functions of the Proton Kinetic Energy ( $y = \log T_p$ ) in TeV.
Nondiffraction, eq. (6)	
$a_0$ .....	$-1.5243(y + 3.3) + 10.107(y + 3.3)^2 - 4.3126(y + 3.3)^3 + 0.80081(y + 3.3)^4 - 0.048724(y + 3.3)^5$
$a_1$ .....	$-2.6297 \times 10^{-5} + 9.3858 \times 10^{-5} \exp[-0.32384(y + 3.4)] + 7.7821 \times 10^{-6}/(y + 4.0560) + 7.6149 \times 10^{-6}y - 8.4091 \times 10^{-6}y^2$
$a_2$ .....	$-223.62 + 59.374y - 5.7356y^2 + 1.9815y^3 - 1.0478y^4$
$a_3$ .....	$0.50807 + 0.60221y + 0.0034120y^2 - 0.011139y^3$
$a_4$ .....	$2.6483(y + 3.32) + 4.4585(y + 3.32)^2 - 1.2744(y + 3.32)^3 - 0.11659(y + 3.32)^4 + 0.0030477(y + 3.32)^5$
$a_5$ .....	$9.1101 \times 10^{-7} + 1.3880 \times 10^{-6} \log[0.016998(y + 4.3)]1.2744 \times 10^{-4}/(y + 4.7707)^2$
$a_6$ .....	$-272.11 - 53.477 \log[0.35531(y + 3.9)] + 56.041/(y - 6.0876)^2$
$a_7$ .....	$6431.8 + 893.92 \log[5.713 \times 10^{-9}(y + 3.9)] + 2103.6/(y + 5.6740) - 6.1125y^2$
$a_8$ .....	$-0.11120 + 0.38144y - 0.040128y^2 + 0.0047484y^3 + 0.0054707y^4$
$r(y)$ .....	$2.56 \exp(-107\{(y + 3.25)/[1 + 8.34(y + 3.25)]\}^2) - 0.385y - 0.125y^2$ for $T_p \leq 15.6$ GeV, 1.0 for $T_p > 15.6$ GeV
Diffraction, eq. (9) <sup>a</sup>	
$b_0$ .....	$70.430 \tanh[-0.35816(y + 2.2)] - 6.6796(y + 0.52273)^2 + 0.0065659(y + 9.5266)^4$
$b_1$ .....	$-8.1145 + 7686.0 \exp(4.4046 \times 10^4\{(y + 2.2190)/[1.0 + 81.105(y + 2.2190)]\}^2)$
$b_2$ .....	$-1.3095 + 0.071270 \tanh[-0.0075463(y + 1.9)] + 0.067759(y + 5.3433) - 0.0044205(y - 1.8683)^2$
$b_3$ .....	$0.082149 - 2190.1 \exp(-533.75\{(y + 2.8363)/[1.0 + 7.0976(y + 2.8363)]\}^2)$
$b_4$ .....	$2.7540 + 0.33859(y + 2.95)^2 - 0.0034274(y + 2.95)^4 + 1.1679 \exp\{-10.408[y + 2.2 - 0.18922(y + 2.2)^2]^2\}$
$b_5$ .....	$2.1817 - 0.59584 \tanh[2.7054(y + 1.9)] - 0.010909 \times (y - 14.9)$
$b_6$ .....	$1.4591 + 1.0275y - 0.074949y^2 - 0.0060396y^3 + 0.0097568y^4$
$b_7$ .....	$3.7609 + 4.2843 \tanh[-0.37148(y + 2.1)] - 0.16479 \times (y - 2.7653)$
$\Delta(1232)$ , eq. (12)	
$c_0$ .....	$2.8262 \exp(-62.894\{(y + 3.1250)/[1.0 - 0.47567(y + 3.1250)]\}^2) + 5.6845 + 13.409/y - 0.097296y^2$
$c_1$ .....	$16.721 + 11.750y + 2.4637y^2$
$c_2$ .....	$-6.0557 - 6.3378 \tanh[21.984(y + 2.1)] + 0.43173y$
$c_3$ .....	$0.37009 + 0.27706y$
$c_4$ .....	$0.047507 + 0.061570y + 0.0070117y^2$
res(1600), eq. (12) <sup>b</sup>	
$d_0$ .....	$2.2400 \exp(-57.159\{(y + 2.9492)/[1.0 + 1.2994(y + 2.9492)]\}^2) - 0.66521 - 0.27554y$
$d_1$ .....	$-7.0650 - 4.2773y - 0.17648y^2$
$d_2$ .....	$-7.0410 - 7.1977 \tanh[31.095(y + 2.1)] + 0.40238y$
$d_3$ .....	$-1.2354 - 0.87581y - 0.20829^2$
$d_4$ .....	$-0.11395 + 0.34418y + 0.27103y^2 + 0.050248y^3$

<sup>a</sup>  $b_0, \dots, b_3 = 0$  for  $T_p < 11.05$  GeV.

<sup>b</sup> Parameters  $c_0, \dots, c_4$  replaced with  $d_0, \dots, d_4$ .

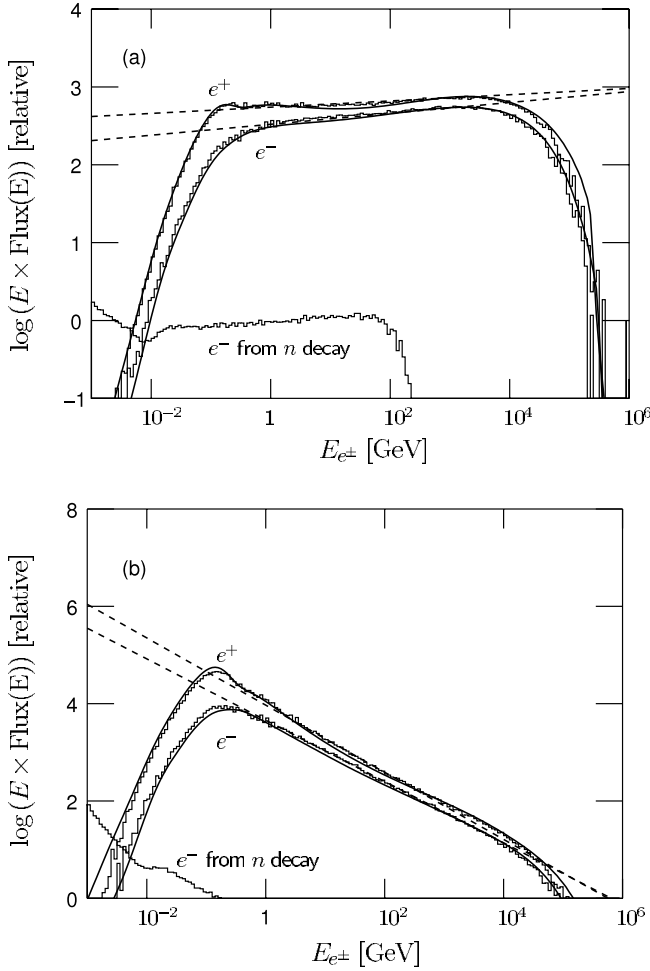


FIG. 12.—Electron and positron spectra produced by protons with power-law spectrum cutoff at  $T_p = 512$  TeV: (a) index = 2 and (b) index = 2.7 by the readjusted model A and by the parameterized model (solid lines) defined by equations (6), (9), and (12). The parameters are defined in Table 4 for electrons and in Table 5 for positrons. The histograms are those of the simulation by the readjusted model A. The dashed straight lines correspond to asymptotic power laws: for electrons 1.93 and 2.63, respectively; and for positrons 1.96 and 2.69, respectively. The histograms in the lower left corner of (a) and (b) show the spectra of the electrons from the neutrons produced by the power-law protons.

### 5.1. Parameterized Gamma Ray Spectrum

The final functional representation of inclusive cross sections for secondary gamma rays is given in equations (6), (9), and (12), with parameters defined as functions of  $T_p$  in TeV (not GeV) in Table 3. The total inclusive gamma-ray spectrum is the sum of the nondiffractive, diffractive, and resonance-excitation contributions. The spectrum produced by protons with a continuous spectrum can be calculated by summing over the total gamma-ray spectra for monoenergetic protons with appropriate spectral weight. For example, the spectra for power-law protons extending to  $T_p = 512$  TeV with index = 2 and 2.7 have been calculated and compared with the corresponding histograms produced from the simulated events in Figure 11. The parameterized model reproduces either spectrum within 10%: it predicts 10%–20% more gamma rays than simulation by the readjusted model A at the higher kinematical limit.

### 5.2. Parameterized $e^\pm$ and Neutrino Spectra

The parameterization has been extended to other secondary particles,  $e^-$ ,  $e^+$ ,  $\nu_e$ ,  $\bar{\nu}_e$ ,  $\nu_\mu$ , and  $\bar{\nu}_\mu$ , in the same way as for

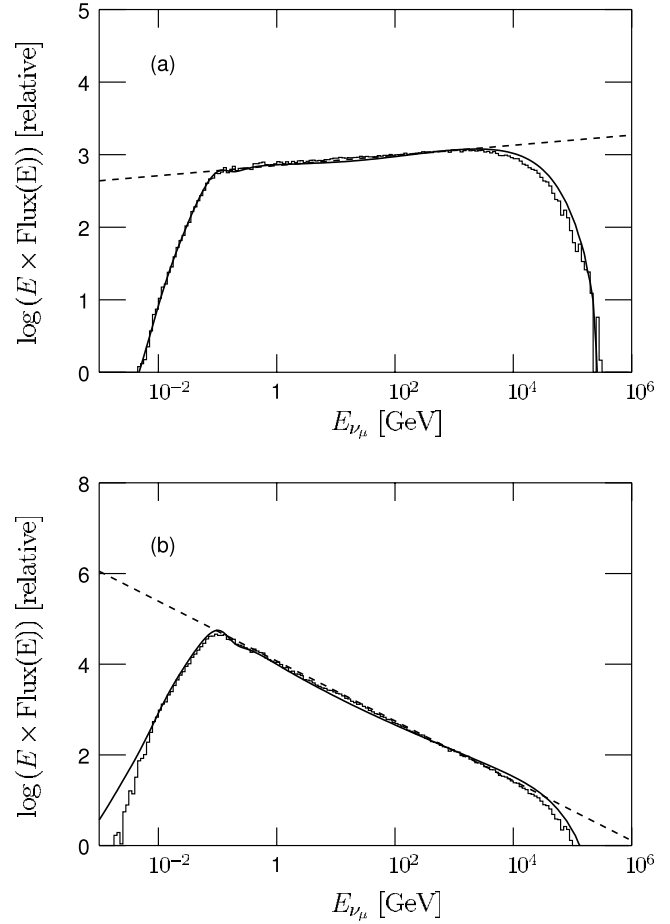


FIG. 13.—Muon neutrino spectra produced by protons with power-law spectrum of (a) index = 2 and (b) index = 2.7 by the parameterized model (solid curves) defined by equations (6), (9), and (12). The parameters are defined in Table 8. The histograms are those of the simulation by model A and  $\Delta$ -excitation. The dashed straight lines correspond to an index of (a) 1.93 and (b) 2.66. Note that the muon antineutrino spectra are the same.

gamma rays. Their functional formulae are represented by equations (6), (9), and (12) with the parameters defined in Tables 4, 5, 6, 7, 8, and 9, respectively. We note that no  $\pi^-$  is produced in  $\Delta(1232)$  decay in readjusted model A and, hence, no  $e^-$  and  $\bar{\nu}_e$  either.

We note that the secondary electron and positron spectra from charged pion and muon decays have been calculated including the polarization effect of the weak interaction theory. The spectra produced by power-law protons of index = 2.0 and 2.7 ( $T_p < 512$  TeV) have been computed based on these parameterized models in Figure 12 for  $e^\pm$  and Figure 13 for  $\nu_\mu$ . We note in Figure 12 that more  $e^+$  are produced than  $e^-$  throughout their spectra. This is largely due to the charge conservation and enhanced by the fact that we have neglected  $\alpha$ -particles and neutron decays. The number of electrons produced in the  $p$ - $p$  interaction will match that of positrons if we include electrons coming out of neutron decays.

For given  $T_p$ , electrons from neutron decays have low energy (mostly with  $E < 10$  MeV), as shown by the lower histograms in Figure 12. They do not contribute to the high-energy gamma-ray spectrum.

## 6. APPLICATION TO GALACTIC DIFFUSE GAMMA-RAY EMISSION

We have replaced the  $\pi^0$  production subroutine of Galprop (Strong & Moskalenko 1997, 2001) with the present parameterized

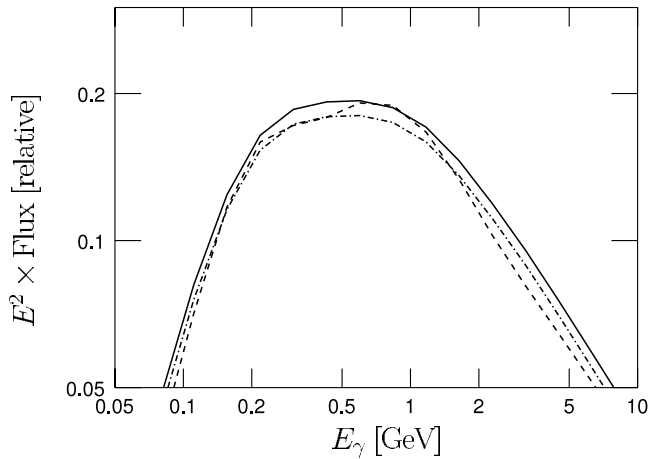


FIG. 14.—The  $\pi^0$  gamma-ray spectra in the Galactic ridge obtained with Galprop with the parameter set, galdef500180: the Galprop built-in  $p$ - $p$  interaction model (dashed line), the present parameterized  $p$ - $p$  interaction model (dash-dotted line), and the present parameterized model normalized to the dashed line in the energy band 0.7–0.8 GeV (solid line).

model and compared the Galactic diffuse gamma-ray spectra of  $\pi^0$  origin with that by the built-in subroutine. A common parameter set, galdef500180 described in Strong et al. (2004), has been used in the two calculations.

As shown in Figure 14, the present parameterized model gives a flatter and smoother spectral energy distribution between  $E_\gamma = 0.3$ – $2$  GeV, smaller gamma-ray yield between  $0.5$ – $1.3$  GeV, and a higher power-law index between  $1$  and  $5$  GeV than the Galprop built-in model. In Kamae et al. (2005), gamma-ray spectrum of the Galprop built-in model was compared with that of model A, after being normalized in the energy range  $E < 300$  MeV. This normalization-enhanced gamma ray yields in the GeV range relative to the sub-GeV range. The Galprop built-in  $p$ - $p$  interaction model has been tuned to reproduce accelerator experiments better than model A of Kamae et al. (2005) near the threshold. We have included the resonance contributions in the present model to improve this shortcoming near the threshold. Hence, we have change the normalization point to the peak region in  $E^2 d\text{flux}/dE$ ,  $E_\gamma = 0.7$ – $0.8$  GeV, where gamma rays from pi-zero decays are expected to dominate (see Fig. 14, dashed curve). The present model thus normalized gives  $\sim 20\%$  higher gamma-ray yield than Galprop at  $2$  GeV: this is substantially lower than the difference (about  $50\%$ ) shown in Figure 7 of Kamae et al. (2005). The gamma-ray power-law index of the present model is harder by about  $0.05$  than that by the Galprop built-in model, just as model A of Kamae et al. (2005) predicts.

## 7. CONCLUSION AND FUTURE PROSPECTS

We have presented the inclusive cross sections of stable secondary particles ( $\gamma$ ,  $e^\pm$ ,  $\nu_e, \bar{\nu}_e, \nu_\mu, \bar{\nu}_\mu$ ) produced by the  $p$ - $p$  interaction in parameterized formulae. They facilitate computation of secondary particle spectra for arbitrary proton spectra as shown for the Galactic diffuse gamma-ray spectrum (Fig. 14). Various effects that these secondary particles may have in astronomical environments can also be calculated at a higher precision. The formulae incorporate all important known features of the  $p$ - $p$  interaction up to about  $T_p = 500$  TeV and hence will also be useful in calculating background when searching for new phenomena.

The parameterized model predicts all secondary particle spectra to have harder power-law indices than that of the incident proton, and their inclusive cross sections to be larger than those expected from the old  $p$ - $p$  interaction models. When used to replace the  $p$ - $p$  subroutine in Galprop (Strong & Moskalenko 1997, 2001), the model gives a flatter spectral energy density distribution between  $0.3$  and  $5$  GeV. The absolute gamma-ray yield predicted by the model is smaller than that by the Galprop model for  $E_\gamma < 1.5$  GeV but higher for  $E_\gamma > 1.5$  GeV. If normalized near the peak in  $E^2 d\text{flux}/dE$  ( $E_\gamma = 0.7$ – $0.8$  GeV), the parameterized model gives a  $\sim 20\%$  higher gamma-ray yield at  $2$  GeV than the model of Galprop: our model with this normalization can account for  $\sim 20\%$ , not  $\sim 50\%$  as was claimed in Kamae et al. (2005), of the discrepancy between the diffuse Galactic ridge gamma-ray spectrum observed by EGRET and model predictions for the proton spectrum near the solar system (the power-law index  $\sim 2.7$ ; Hunter et al. 1997). We note the discrepancy will be reduced by inclusion of the inverse Compton component (see, e.g., the model by Strong et al. 2004).

The present model also predicts more  $e^+$  than  $e^-$  at higher energies wherever those produced by the  $p$ - $p$  interaction become comparable in flux to primary  $e^-$  and  $e^+$ . The formulae and parameters given in the tables are available as supplementary online material both in C language format and as C subroutine. We are currently parameterizing the angular distribution of gamma rays relative to the incident proton direction. The results will be published elsewhere.

The authors would like to acknowledge valuable discussions with and comments received from M. Asai, E. Bloom, P. Carlson, J. Chiang, J. Cohen-Tanugi, S. Digel, E. do Couto e Silva, I. Grenier, G. Madejski, I. Moskalenko, P. Nolan, O. Reimer, D. Smith, F. Stecker, A. Strong, H. Tajima, and L. Wai. They also wish to thank the anonymous referee for valuable comments and suggestions and John Houck for suggestions to improve C codes.

## REFERENCES

- Aharonian, F. A. 2004, Very High Energy Cosmic Gamma Radiation: A Crucial Window on the Extreme Universe (World Scientific Publishing)  
 ———. 2005, *Science*, 307, 1938  
 Aharonian, F. A., Völk, H. J., & Horns, D. 2004a, Proc. Int. Symp. on High Energy Gamma-Ray Astronomy (Singapore: World Scientific)  
 Aharonian, F. A., et al. 2004b, *Nature*, 432, 75  
 ———. 2004c, *A&A*, 425, L13  
 Berezhko, E. G., & Völk, H. J. 2000, *ApJ*, 540, 923  
 Blattnig, S. R., et al. 2000, *Phys. Rev. D*, 62, 094030  
 Bloemen, J. B. G. M. 1985, *A&A*, 145, 391  
 Bloemen, J. B. G. M., et al. 1984, *A&A*, 135, 12  
 Böttcher, M., & Reimer, A. 2004, *ApJ*, 609, 576  
 Crawford, J. F., et al. 1980, *Phys. Rev. C*, 22, 1184  
 Dermer, C. D. 1986a, *A&A*, 157, 223  
 ———. 1986b, *ApJ*, 307, 47  
 DuVernois, M. A., et al. 2001, *ApJ*, 559, 296  
 Enomoto, R., et al. 2002, *Nature*, 416, 823  
 Hagiwara, K., et al. 2002, *Phys. Rev. D*, 66, 010001  
 Halzen, F., 2005, in AIP Conf. Proc. 745, Second Int. Symposium on High Energy Gamma-Ray Astronomy, ed. F. A. Aharonian, H. J. Völk, & D. Horns (New York: AIP), 3  
 Hayakawa, S. 1969, *Cosmic Ray Physics* (New York: Wiley)  
 Hunter, S. D., et al. 1997, *ApJ*, 481, 205  
 Iyudin, A. F., et al. 2005, *A&A*, 429, 225  
 Kamae, T., Abe, T., & Koi, T. 2005, *ApJ*, 620, 244  
 Katagiri, H., et al. 2005, *ApJ*, 619, L163  
 Koyama, K., et al. 1997, *PASJ*, 49, L7  
 Mårtensson, J., et al. 2000, *Phys. Rev. C*, 62, 014610  
 Mayer-Hasselwander, H. A., et al. 1982, *A&A*, 105, 164  
 Mori, M. 1997, *ApJ*, 478, 225

- Mücke, A., & Protheroe, R. J. 2001, *Astropart. Phys.*, 15, 121
- Mücke, A., et al. 2003, *Astropart. Phys.*, 18, 593
- Müller, D. 2001, *Adv. Space Res.*, 27, 659
- Murthy, P. V. R. and Wolfendale, A. W. 1986, *Gamma-Ray Astronomy* (Cambridge: Cambridge Univ. Press)
- Ong, R. A. 1998, *Phys. Rep.*, 305, 93
- Schlickeiser, R. 2002, *Cosmic Ray Astrophysics* (Berlin: Springer)
- Schönfelder, V., ed. 2001, *The Universe in Gamma Rays* (Berlin: Springer)
- Sjöstrand, T., Lonnblad, L., & Mrenna, S. 2001, *Pythia 6.2: Physics and Manual* (Lund Univ. Rep. LU-TP 01-21), hep-ph/0108264
- Sjöstrand, T., & Skands, P. Z. 2004, *J. High Energy Phys.*, 3, 53
- Slane, P., et al. 1999, *ApJ*, 525, 357
- Stanev, T. 2004, *High Energy Cosmic Rays* (Berlin: Springer)
- Stecker, F. 1970, *Ap&SS*, 4, 377
- . 1971, *Cosmic Gamma Rays* (NASA SP-249; Greenbelt: NASA)
- . 1973, *ApJ*, 185, 499
- Stecker, F. 1990, in *Cosmic Gamma Rays, Neutrinos, and Related Astrophysics*, ed. M. M. Shapiro & J. P. Wefel (Dordrecht: Kluwer), 89
- Stephens, S. A. 2001, *Adv. Space Res.*, 27, 687
- Stephens, S. A., & Badhwar, G. D. 1981, *Ap&SS*, 76, 213
- Strong, A. W., & Moskalenko, I. V. 1997, in *AIP Conf. Proc. 410, Fourth Compton Symp.*, ed C. D. Dermer, M. S. Strickman, & J. D. Kurfess (New York: AIP), 1162
- . 2001, in *Proc. 27th Cosmic Ray Conf. (Hamburg)*, 1942
- Strong, A. W., Moskalenko, I. V., & Reimer, O. 2000, *ApJ*, 537, 763 (erratum 541, 1109)
- . 2004, *ApJ*, 613, 962
- Strong, A. W., et al. 1978, *MNRAS*, 182, 751
- . 1982, *A&A*, 115, 404
- Tsunemi, H., et al. 2000, *PASJ*, 52, 887
- Uchiyama, Y, Aharonian, F. A., & Takahashi, T. 2003, *A&A*, 400, 567
- Weekes, T. C. 2003, in *Proc. 28th Int. Cosmic Ray Conf. (Tsukuba)*, 3